UNIVERSITAT POLITÈCNICA DE VALÈNCIA

School of Design Engineering

Design and Testing of a Parachute Recovery System for a
Sounding Rocket Experiment

End of Degree Project

Bachelor's Degree in Aerospace Engineering

AUTHOR: Albiñana Burdiel, Carlos

Tutor: Tiseira Izaguirre, Andrés Omar

Cotutor: Gil Megías, Antonio

ACADEMIC YEAR: 2021/2022

UNIVERSITAT POLITÈCNICA DE VALÈNCIA

School of Design Engineering

DESIGN AND TESTING OF A PARACHUTE RECOVERY SYSTEM FOR A SOUNDING ROCKET EXPERIMENT

END OF DEGREE PROJECT
Bachelor's Degree in Aerospace Engineering

AUTHOR
Carlos Albiñana Burdiel

TUTOR
Prof. Andrés Omar Tiseira Izaguirre

COTUTOR
Prof. Antonio Gil Megías

ACADEMIC YEAR: 2021/2022

Design and testing of a parachute recovery system for a sounding rocket experiment

Carlos Albiñana Burdiel

Abstract

The following End of Degree Project presents the theory and modelling behind the design of parachute recovery systems for airborne vehicles, with special emphasis on its use for Sounding Rockets. The aim of this work is to explain how this theory is applied to the construction of a Dual Deployment Parachute Recovery System for a 3 km Solid Boosted Sounding Rocket. This rocket will compete on the 2022 edition of the European Rocketry Challenge *EuRoC*.

Special attention was given to the Parachute Opening Force estimation, using both modern semi-empirical approaches like Moment-Impulse Theorem as well as more established models in the likes of Pflanz method. These physical models and semi-empirical approaches have been used to determine the final design. This document also proves the validity of said theory when applied to smaller airborne vehicles. All the subsystems that form the recovery system were tested and positively evaluated through the means of drop testing, ground testing and breaking strength analyses. This recovery system has been validated with the launch of a 1 km apogee sub-scale prototype. As such, a suitable hot gas deployment and dual recovery system is found.

Key Words: Parachute Recovery, Sounding Rocket, Parachute Inflation, Opening Force, Snatch Force, Dual Deployment.

Diseño y ensayo de un sistema de recuperación mediante paracaídas para un cohete sonda experimental.

Carlos Albiñana Burdiel

Resumen

Este Trabajo de Final de Grado expone la teoría y modelos físicos que permiten el diseño de sistemas de recuperación por paracaídas en vehículos aéreos, con especial énfasis en su aplicación en cohetes sonda. El propósito es explicar cómo se ha hecho uso de esta teoría para la construcción de un sistema de recuperación en dos etapas para un cohete sonda experimental con motor sólido de 3 km de apogeo. El cohete competirá en la edición de 2022 del concurso de cohetería europeo *EuRoC*.

Se presta particular atención a la estimación de fuerzas de apertura del paracaídas, utilizando tanto métodos semiempíricos modernos, como el Teorema de Momento-Impulso, así como procedimientos más establecidos como el Método de Pflanz. Estos modelos físicos y medianos semiempíricos han sido utilizados para la realización del diseño final del sistema de recuperación. El trabajo muestra a su vez la validez de aplicar estos métodos a vehículos aéreos ligeros. Todos los subsistemas han sido comprobados mediante ensayos en tierra, lanzamientos y análisis de esfuerzos mecánicos. El sistema de recuperación ha sido validado con el lanzamiento de un prototipo subescala de 1 km de apogeo. De este modo, se ha encontrado un sistema eficaz de eyección por pólvora de un sistema de recuperación en dos etapas para un cohete sonda.

Palabras Clave: Recuperación por Paracaídas, Cohete Sonda, Hinchado de Paracaídas, Fuerza de Apertura de Paracaídas, Fuerza de Reaceleración de Paracaídas, Recuperación en dos etapas.

Disseny i prova d'un sistema de recuperació mitjançant paracaigudes per a un coet sonda experimental

Carlos Albiñana Burdiel

Resum

Aquest Treball de Final de Grau exposa la teoria i models físics que permeten el disseny de sistemes de recuperació per paracaigudes en vehicles aeris, amb especial èmfasi en la seua aplicació en coets sonda. El propòsit és explicar com s'ha fet ús d'aquesta teoria per a la construcció d'un sistema de recuperació en dues etapes per a un coet sonda experimental amb motor sòlid de 3 km d'apogeu. El coet competirà en l'edició de 2022 del concurs de cohetería europeu *EuRoC*.

Es presta particular atenció a l'estimació de forces d'obertura del paracaigudes, utilitzant tant mètodes semiempírics moderns, com el Teorema de Moment-Impuls, així com procediments mes establerts com el Mètode de Pflanz. Aquests models físics i mitjans semiempírics han estat utilitzats per a la realització del disseny final del sistema de recuperació. El treball mostra al seu torn la validesa d'aplicar aquests mètodes a vehicles aeris lleugers. Tots els subsistemes han estat verificats per mitjà de proves en terra, llançaments i anàlisis d'esforços mecànics. El sistema de recuperació ha estat validat amb el llançament d'un prototip subescala d'1 km d'apogeu. D'aquesta manera, s'ha trobat un sistema eficaç d'ejecció per pólvora d'un sistema de recuperació en dues etapes per a un coet sonda.

Paraules Clau: Recuperació per Paracaigudes, Coet Sonda, Inflat de Paracaigudes, Força d'Obertura de Paracaigudes, Força de Reacceleració de Paracaigudes, Recuperació en dues etapes.

Dedication

I dedicate my final degree project to my good friends and colleagues at my University Rocketry Team: *Faraday Rocketry UPV*, who enabled me to begin my journey into becoming what many kids dream of: Being a Rocket Scientist.

I would also love to dedicate my work to my high school physics and math teachers: Miguel Roca and Luis Mayor. They made me fall in love with science again.

Last but not least, to my good friend Arturo.

Declaration

I hereby declare that this end of degree project represents my own work and has not been previously included in any form of academic work submitted to this University or any other institution. The experimental work is almost entirely my own work; the collaborative contributions have been indicated clearly and acknowledged.

Certain materials are included under the fair use exemption of the U.S. and E.U Copyright Law and have been prepared according to the fair use guidelines and are restricted from further use.

Acknowledgements

Contents

List of Figures

List of Tables

Introduction

The term *Recovery* is defined as "the action or process of regaining control" and "a return to a normal state". In engineering, this constitutes the study of systems that allow a target to be reclaimed or to retrieved. In this sense, various recovery models have emerged throughout history, all with the same basic purpose: Lower the velocity of the target and provide a safe landing. Parachute recovery refers to the use of an aerodynamic decelerator system as a means of decreasing the rate of descent sufficiently until said landing can be achieved. Earliest depiction of what can be described as a parachute can be traced back to 2000 B.C in ancient China, where Chinese historian Sima Qian describes the legend of a king escaping death by jumping with a bamboo hat [1]. Leonardo da Vinci in 1485 would famously portray several flying machines along with what can be confidently described as a pyramid shaped parachute. It will not be until the First World War when parachutes began to be developed for pilots and airdrops.

Nowadays, parachute recovery is most commonly used, but not limited to, the retrieval of airborne vehicles, airdrops of personnel and cargo (whether it be it in emergency or planned missions), ordnance retardation and sport/recreational parachuting. However, the use of these systems can also be found in the landing procedure of some heavy vehicles, most notably the Boeing B-52H *Stratofortress* or the Space Shuttle, along with the emergency termination of dangerous aircraft maneuvers. This include spin and deep stall recovery [2].

This project focuses on the parachute recovery of sounding rockets for professional builds as well as looking into hobbyists and amateur rocketry, in the so called *HPR* (High Power Rocketry) scene. Moreover, a parachute recovery design is proposed and evaluated for a 3 km apogee rocket for the University Team *Faraday Rocketry UPV*. The system includes a student built stage separator and will serve as a basis for all future recovery system developed by this team.

Chapter 1

Parachute Recovery Definitions and Parameters

1.1 Recovery Model and Design Considerations

Recovery System is a term that encompasses many design stages and subsystems within a mission or assembly. This includes any stage with the purpose of safe retrieval of the target. These subsystems can deal with impact attenuation, flotation, docking, sequencing, location and, of course, parachute recovery [2]. This work focuses on the latter. In order to avoid confusion, any mention of the term *Recovery System* onward will be exclusively referring to the Parachute Recovery Subsystem.

The type of recovery system used is highly dependant on the requirements of the mission. For instance, the ability of reusing a parachute system in spacecraft landing or ordnance makes no sense from a design perspective. However, reusability is of utmost importance in aircraft landing. A comparative rating for different applications can be seen in Table 1.2.

Moreover, on top of the nature of the mission, there are many factors that will contribute to the design considerations of a parachute system. These design criteria add an additional layer of complexity to the planning phase. In addition to the performance characteristics listed in Table 1.2, the most significant parameters are noted in Table 1.1 [3]. Therefore, recovery engineers must take these parameters into consideration, decide which are most critical for the mission and aim to design the most well rounded system suited for the project.

Reliability	Stability	High Drag
Low Opening Shock	High Mach Capability	Repeateable Performance
Envirnomental Adaptabilty	Damage Resistance	Simplicity of Design
Simplicity of Service	Low Acquisition Cost	Low Life Cycle Cost
Weight Efficiency	Volume Efficiency	Cost Efficiency
Parachute Drag Area	Parachute Weight	Parachute Volume

Table 1.1: Design Criteria for Parachute Recovery Systems

Performance characteristics	Application					
	Spacecraft Landing	Airborne Troops	Aircraft Escape	Aircraft Landing Deceleration	Ordnance	Aerial Resupply
Reliability	3	3	3	2	3	2
Repeateability of performace	2	2	2	3	3	1
Reuseability	0	3	0	3	0	3
Low Weight and Volume	3	2	3	2	2	1
Stability	2	2	2	3	3	2
High Drag	2	2	2	2	2	3
Low Opening Forces	1	3	2	3	2	3
Low maintenance	1	3	2	3	2	3
Cost	1	2	2	2	2	3

Table 1.2: Comparative Rating for various parachute recovery system applications. Rating varies from 3 to 0 in a scale of 'high importance' to 'not applicable'

Evidently, *Reliability* will virtually always stand on top of the list for any engineering project. Particularly in Parachute Recovery, failure of any subsystem can lead to catastrophic consequences. The risk of an unreliable performance is usually mitigated with the use of redundant systems. While it is true that there have been many efforts in incorporating redundant procedures within the recovery stage, the actual parachute system as a whole is rarely accompanied by a backup parachute, except for airborne troops or recreational parachuting. [2]

Stability and *Steady State Descent* also play a key role in the selection of any parachute system. The main course of action is usually the estimation of an optimal terminal velocity window, whereby the calculation of the rest of parameters revolve around this target. In addition, the system is always scaled to offer a suitable degree of stability that will dampen oscillations during deployment and descent.

Moreover, low *Volume* and *Weight* are frequently desired. As these parameters often come in pairs when dealing with parachute systems, the terms *Packing Volume* and *Packing Pressure* are commonly used. Packing volume wants to be maximized, as the decrease of volume of the packed system will allow less restrictive recovery bay areas within the deployment section. However, parachutes will have a maximum allowed packing density. If said parameter is too high, it will not allow proper inflation. The system may not even unroll correctly in the deployment stage, leading to higher than estimated filling speeds which will cause excessive forces on both the chute canopy and axial stress on the parachute lines. [3] [4]

The term *Parachute Drag Area* refers to the product of the area of the parachute and its drag coefficient C_D, often written as $(SC_D)_0$. This term is needed for the calculation of the terminal velocity of the system. The sub-index denotes the specific drag area in question. This will be explored in Section 1.2.1. It is also linked to the *Weight*, *Volume* and *Cost efficiency*, whereby the drag area is divided by these parameters to obtain the respective efficiency.

Lastly, the remaining parameter that demands clarification is the *Low Opening*

Shock. When deploying a parachute, the rapid inflation of the system causes a fast increase in $(SC_D)_0$. There will be a point at which the forces acting on the system is highest. The term referring to the forces that the parachute must be able to sustain is called *Canopy Loading* and will be further explained in Section 2.3.1. In short, the lower the load, the less stress is placed on the system, thus allowing for less reinforced textiles, which add complexity and weight to the structure.

1.2 Parachute

1.2.1 Parachute Parameters

Even though there are many parachute types (see Section 1.2.2), they all contain the basic elements shown in Figure 1.1. The *canopy* is comprised of a number of tapered or triangular cloth *gores*, sewn together in a circumferential pattern and bounded by the *skirt band* and the *vent band* at the outer and inner sections respectively. This element inflates with the flow of air and generates the necessary forces for deceleration and balance of the falling system.

The *skirt* refers to the outermost section of the canopy that forms the leading edge of the parachute. The extension of this element provides increased stability and decreases shock loading during the inflation process [2]. The remaining section

Figure 1.1: Main Parts of a Parachute [2]

of the canopy is known as the *crown*. The small circular opening located at the *apex* of the canopy is known as the *vent* and it is only a small percentage of the canopy area [2]. This element serves two purposes: It simplifies manufacturing and the sewing of the gores as well as provides stress relief during the inflation process, allowing some mass flow through and minimizing the pressure differential. Regardless of canopy shape, it is a necessary component that improves parachute performance. [5]

The *suspension lines* transmit the drag force from the canopy to the body meeting at the *confluence point*. It is then transmitted through a cord known as the *riser* to the rest of the structure or body. The length of suspension lines from the skirt to the confluence point is regarded as the *effective suspension line length l_e*. This parameter greatly impacts the shape the canopy will adopt, thus making the ratio $\frac{l_e}{D_0}$ an important design parameter and usually ranges from 0.8 to 1.25 [2].

A distinction is made between the dimensions of projected canopy shape and the actual parachute surface area. The maximum cross-sectional area of the inflated concave canopy is regarded as the Projected Surface Area S_p with its subsequent Projected Diameter D_p. On the other hand, the total cloth surface used in the

Figure 1.2: Parachute Dimensions

construction of the parachute is named the Nominal Surface Area S_0, with the analogous Nominal Diameter D_0. Also, as a side note, it must be stated that the Drag Coefficient Cd is usually calculated with the parameter S_0, thus forming the term $(SCd)_0$. However, one can find instances of the Cd being related to the S_p. This yields higher that expected Cd values and special care must be taken when dealing with parachute manufacturers in order to properly size the recovery system.

Finally, as a means of allowing for faster slow-speed inflation time, some parachutes are constructed with a *Pull Down Vent Line*. This consists of an inner line attached to the vent which connects to the rear risers of the system. The vent is pulled inwards slightly above the skirt level. The canopy then adopts a sort of toroidal shape, also increasing the Cd. This parachute is often referred as a *Pull Down Apex Parachute* [2].

1.2.2 Parachute type

There are numerous parachute shapes and configurations. Their characteristics depend on the specific purpose within the mission. Furthermore, several iterations have been proposed and developed along the years to combat certain issues within aerodynamic decelerators, be it high opening forces, low stability or low weight efficiency by means of particular inflated profiles, mouth and vent gaps and material selection. In rocketry, recovery is performed typically in two descent stages. The different purpose of these phases demand the use distinct parachutes configurations. A table containing the most common parachute types with their respective parameters can be seen in Appendix G. A great explanation on how these several configurations are constructed can be found in Reference [2].

The parachute stages are divided in this document into Drogue and Main Parachute. However, Pilot or Extractor Chutes are also relevant to rocket recovery and they are used as an auxiliary system to pull on and deploy the subsequent bigger parachute. Nonetheless, Drogue Parachute are frequently used as Pilot Chutes on top of their usual purpose. Figure 1.3 shows the usual rate of descent of different parachute applications.
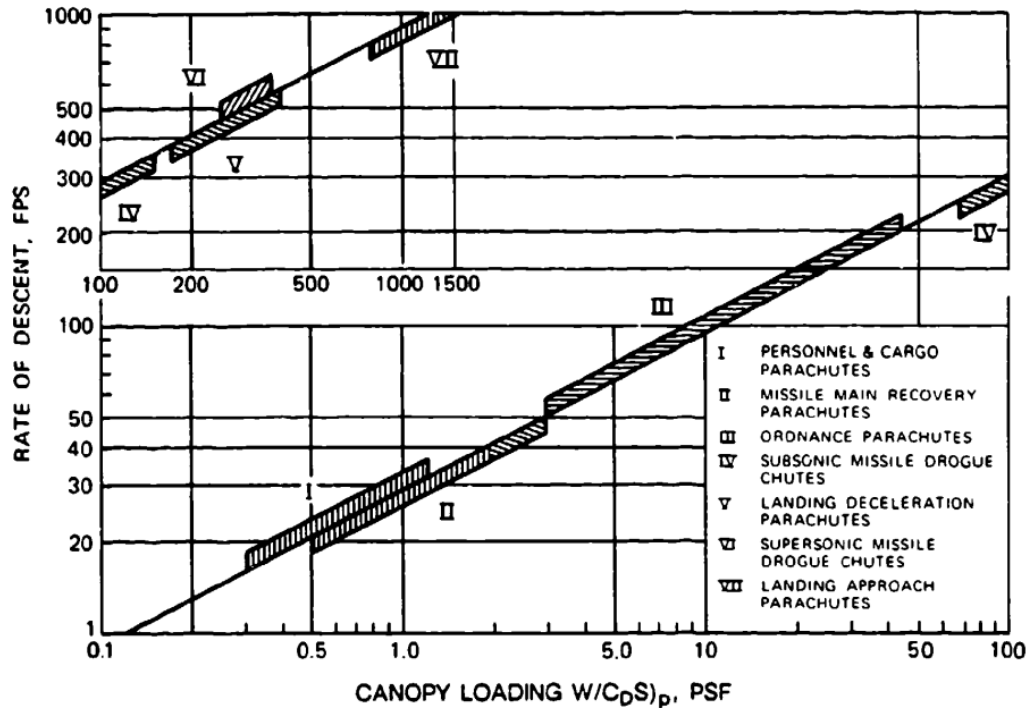
Figure 1.3: Rate of Descent Profile Versus Canopy Loading for various Parachute Applications [3]

1.2.2.1 Pilot and Drogue Chutes

As rockets and other vehicles reach higher apogees, the speed at which the aerodynamic deceleration occurs scales up significantly, greatly impacting the forces the parachute will sustain during inflation. As a result, virtually all High Power Rocket systems will use Pilot or Drogue Chutes in their initial recovery phase. These elements slow down the vehicle to a more controlled terminal velocity, as well as provide initial stabilization to allow a better guided Main Parachute Deployment.

Not only does the staging of the recovery phase limit the peak loading on these decelerator systems, it is also of utmost importance when dealing with the system's drift. If a single stage parachute were to be deployed at a significant altitude, the descending flight time would be substantial. Crosswind is then able to drag the falling system far away from the controlled landing space or area. As a result, having the vehicle fall at a much faster initial rate limits the time the crosswind is able to drift the system away. In the *High Power Rocketry* scene, this staging is referred as *Dual Deployment Recovery*.

1.2.2.2 Main Parachutes

Once the Drogue Chute has lowered the vehicle to the desired altitude, a much larger Main Parachute is deployed to safe land the system at a reasonable terminal and impact velocity. The lateral drift generated by these elements is much higher than in the initial phase. However, as these elements are deployed at a lower controlled altitude, the distance covered is significantly reduced.

1.2.3 Reefing

With the aim of reducing stress on the decelerator systems, the opening and inflation sequence of a single parachute can be separated into incremental stages. Usually, by means of a pyrotechnic line cutter mechanism, a cord prevents the full inflation of the canopy by constraining the mouth opening area. Therefore, the vehicle decreases to a lower dynamic pressure, allowing an inflation process at lower terminal velocity. It also serves to prevent and control overinflation of parachutes, which is a common source of peak stresses in the cloth and lines in larger systems [3].

(a) Reefed Configuration   (b) Final Inflation Configuration

Figure 1.4: Space-X Mark 3 Cluster Parachute Drop Test

1.2.4 Parachute Cluster

Several smaller parachutes can be deployed together in a *cluster* configuration to stabilize and lower the vehicle to the desired terminal velocity. These systems offer a higher degree and window of stability and are easier to store, manufacture, rig and handle than their single large counterpart [3]. Moreover, a cluster configuration is less susceptible to catastrophic failure, as the loss of a small parachute does not necessarily equate to total recovery failure. However, the drag area relationship is not linear. This is, both the angled mouth area and the interference of the airflow between the different parachutes generate drag losses [6][7].

Also, special care must be taken in the rigging system design to prevent suspension line tangling and uneven inflation of parachutes. It is virtually impossible to ensure that all parachute inflate evenly at the same time. Some parachutes will inflate faster than others, leading to higher stress. As determining which one will suffer higher loads is impossible, the individual system for all parachutes must be sized to be able to withstand the maximum estimated load. This overestimation demands stronger cords and connectors which leads to higher recovery weight.

1.3 Recovery Lines

The term *recovery lines* encompass all cord and connection elements that secure the parachute to the anchor point of the vehicle. Just like the parachute itself, these must comply with their respective specification guidelines to ensure they will work as intended. Commercial systems for *High Power Rockets* are not required to adhere to the most strict guidelines as long as the competent authority approves their usage. The most common is the *MIL-SPEC* system under the American *Federal Aviation Administration* supervision and professional Sounding Rockets must follow these restrictions [8].

The suspension lines meet at a confluence point with the respective designed suspension line length l_e. These then attach through a connector link, typically a *swivel link* - see Figure 1.6 -, to the rest of the lines of the system. The parachute must be distanced from the

Figure 1.5: Parachute Lines and Cords [2]

hanging body in order to minimize the wake body effects on the surrounding airflow, which will cause instabilities and drag losses on the parachute [9]. This determines the steady state parachute stability, further discussed in Section 2.1. The body-parachute separation is achieved by a long *riser* cord which links the aforementioned connector link to the body. In rocketry, these cords are manufactured as slings to simplify the rigging process with the use of *quick links*. In smaller less professional builds, a knot is sufficient to attach the ends of these lines. However, knots weaken the rope due to the high degree of curvature under stress [10]. As a result, slings are sewn at each end. Even though the sewing process also debilitates the cord's strength, it does so to a lesser degree.

The *bridle* that can be seen in Figure 1.5 is a smaller cord designed to pull on the canopy of the main parachute from the pilot or drogue chute. This way, the pilot chute is able to extract and assist in the deployment of the subsequent decelerator. The bridle length affects the deployment and inflation process of the canopy, thus, parachute manufacturers will establish an optimal bridle length [8]. This cord must not be confused with the inner bridle of a parachute, used to pull down on the apex of the canopy for faster inflation (see Section 1.2.1).

As for the connectors between cords, with the intention of simplifying the information given in this document, only the most conventional and wide-spread elements used in *HPR* systems are discussed below, these being *quick links* and *swivel links*. An in depth analysis and compilation of these components can be found in Reference [8].

(a) Quick Link [8]

(b) Swivel Link

Figure 1.6: Metal Recovery Connectors

Quick Links are elements used for aiding and simplifying the rigging and swapping process of the recovery system. These are often made out of stainless steel and the engineer will chose the appropriate size based on the weight limitation and strength constraint.

On the other hand, *Swivel Links* prevent tangling and keep the parachute mouth open. If a single or several suspension lines are not of equal length, it is possible for the parachute to start rotating. This rotation will twist the lines, essentially decreasing the suspension line length l_e and closing the parachute mouth, greatly impacting the drag the chute is able to generate. These connectors allow rotation of the parachute and eliminate parachute tangling.

Finally, both cord and connector elements have a designed *Safe Working Load (SWL)* and its associated *Safety Factor (SF)*. The *Minimum Breaking Strength* is the average maximum load needed to break the device. Manufacturers, based on their own criteria and/or following their respective consumer safety guidelines, divide this value by the *SF* to obtain a *SWL*. This way, if the Recovery Weight must be lowered, it is possible to test the breaking strength of these elements and use lower rated equipment on the parachute assembly.

1.3.1 Stage Separation and de-rigging

In a broader sense, *Stage Separation* may refer to any moment at which there is a physical disconnection between sections of a rocket, often alluding to different booster stages in the ascending phase. However, *Stage Separation* in this context refers to the moment at which the final descent phase takes place with the deployment of the Main Parachute.

More often than not, amateur *HPR* systems aim to simplify this procedure by constructing the rocket in 3 sections, whereby the Main and Drogue Parachute are housed in separate areas of the rocket. This is seen in Figure 1.7. The parachute stages then split up with a pyrotechnic ejection (See Section 1.4). However, some *HPR* systems dwell into the construction of more professional builds that use a deployment bag with both parachutes contained in the same recovery area [1].
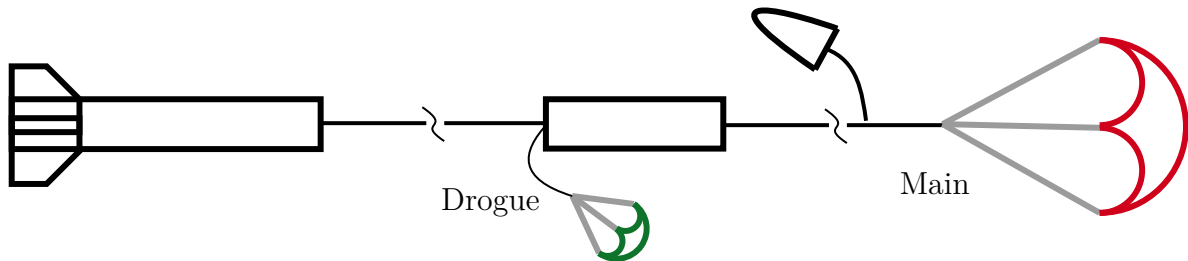
Figure 1.7: Conventional *HPR* Dual Deployment Configuration.

The deployment bag system is the most used method of parachute deployment for sounding rockets, where the drogue parachute or a secondary pilot chute pulls on the main bag when the second recovery phase conditions are met. The procedure to initiate the stage separation is most triggered by *quick-disconnects* elements that may be mechanical, electrical or pyrotechnic in nature, or a combination o several [2]. Most notably, the *line-cutter* mechanism severs the line holding the main parachute bag. This small element uses a pyro-activated sharp blade to cut the cord passing through it.

As rockets grow in size, so does the mechanical requirements and the loads the recovery system is subjected to. These bigger and thicker recovery lines become harder to sever using a simple line-cutter. Therefore, an additional component that uses mechanical advantage to lower the output force is implemented. This way, a smaller line-cutter can sever the lighter cord holding the multiplying system. Some university rocketry teams have implemented their own version of a mechanical advantage separator, mostly based on a simple *3-ring release system*. In Section 4.2.4 an own version of this system is developed for the *Faraday Rocketry* Sounding Rocket.

Also, commercial *HPR* pyro-disconnects have been developed. For instance, *Tinder Rocketry* © offers their so-called *Tender Descenders*, where a small black powder

---

[1]This does not necessarily mean that the drogue and main deployment bag are housed in the exact same compartment. Some systems hold the main chute in a separate hatch but below the drogue parachute anchor point, such as the *Miura 1* rocket [11]

charge is used to forcefully separate the system that holds a parachute line together. Furthermore, several alternatives have been proposed throughout recent years with the booming of Rocketry Divisions at University Levels, as aspiring engineers design new methods for stage separation.

A noteworthy solution that utilizes mechanical advantage is the *Main Chute Release System (MCRS)* designed and implemented by the Norwegian Team *Propulse NTNU*. Two redundant and independent servo motors mounted on steel plates rotate and release the quick link holding the parachute shock cord. It also serves as a fastening point, as the parachute opening load is endured by the double arm system with its mechanical advantage.
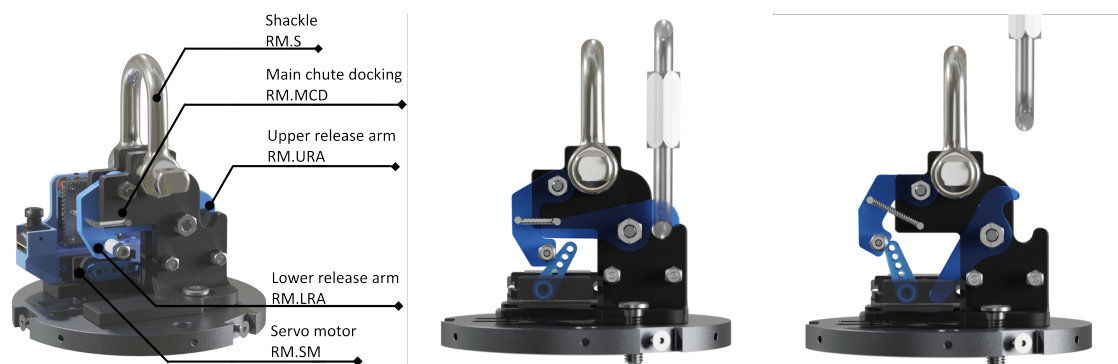
Figure 1.8: MCRS overview (left), MCRS locked position and MCRS open position (right). Image provided by Propulse NTNU

1.4 Deployment

The Recovery Stage of a mission begins with the deployment procedure. The whole parachute system must remain secured to the vehicle and only initiate its action when the avionics subsystem deems it necessary. This is a very critical stage and special care must be taken when manufacturing the space that will house the recovery system. High deployment speeds can easily tear through the thin parachute fabric if any protruding or sharp elements are present. There are several deployment mechanism used in high power rockets, with varying complexity and action principles depending on the deployment conditions and mass of the system. In more amateur *HPR* builds, the recovery system is ejected close to apogee to reduce the speed of inflation of the parachute(s) to minimize the forces on the recovery system. This is not possible as altitude increased due to the surge in drift when descending. A comparative rating for the different deployment mechanism explained below can be seen in Table 1.3.

The parachute must be effectively separated from the vehicle to allow clean air to inflate the canopy. The general rule of thumb is to eject the recovery system with cords of total length of three to four times the rocket length [3]. Reference [12] very effectively describes and summarises the deployment methods implemented in *HPR* builds. These are divided into push and pull categories and may refer to both the payload ejection and/or the recovery system deployment.

Deployment System	Complexity	Max. Rocket Size	Weight	Reaction Load	Ejection Velocity
Hot Gas	1	1	1	2	3
Cold Gas	1-2	2-3	1-2	2	3
Spring	2	1	2	2-3	1-2
Mortar	4	5	5	5	4-5
Slug Gun	4	5	3-4	2-3	4-5
Tractor Rocket	4	5	2	1	4-5
Pilot Chute	1-2	5	2	1	1-5

Table 1.3: Comparative Rating of different Rocket Deployment Mechanisms. Rating varies from 1 to 5 in a scale of 'Very Low' to 'Very High'

Pyrotechnic ejection (labeled as hot gas in Figure 1.9) has been the staple for model and high power rocketry due to its low cost and weight and simple rigging. A small black powder charge is ignited by the avionics system. The generated gasses pressurize the recovery base and forcefully expel the parachute and its cords outside the rocket. Fireproof and fire-retarding agents and blankets are used to protect the recovery system from these gasses and have proven to work on mid-sized and rockets. This method, however, is not suitable for bigger rockets. Larger recovery bay areas will require more black powder to eject the higher parachute mass. This generates more hot gasses that can easily burn through the thin parachute cloth even with the help of these protecting elements. Evidently, cords that cannot be effectively shielded are made out of Kevlar due to is fire resisting properties.
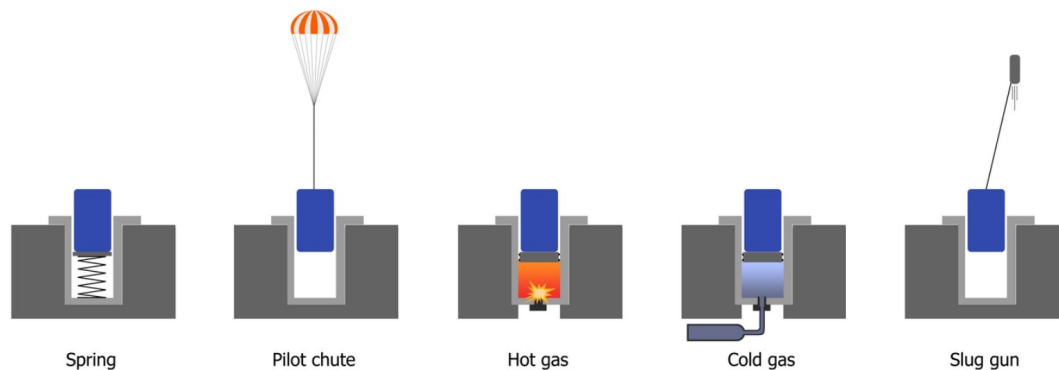
Figure 1.9: Most common deployment mechanisms [12]

Smaller rockets can also use spring-loaded systems, with servo or pyro activation, to eject the parachute. These have the obvious drawback of being susceptible to early release due to the vibrations of the motor.

To combat the negative side effects of hot gas ejection, it is possible to generate this ejecting pressure through the use of pressurized gas canisters. Even commercial systems have been developed that utilize common CO_2 cartridges with simple servo or pyro activated gas release mechanism, such as the the *Peregrine* and *Raptor* system from *Tinder Rocketry* ©. Bigger rockets may also use a mortar system to eject the parachute. However, this technology is very heavy and generates a big kick-back that needs to be accounted for.

(a) *RAPTOR CO2 Ejection System*

(b) The Exhaustless Peregrine

Figure 1.10: *Tinder Rocketry* $^{©}$ CO_2 ejection systems

As for pulling systems, when parachutes become much larger, engineers can use a pyro ejected slug that will pull on the apex of the parachute(s), which substantially reduces kick-back. The constant pull on the chute is also less straining on the cloth than a sudden push. Another alternative is a small tractor rocket, which are normally used for seat ejection and spin stabilization [3]. Finally, an aerodynamic deployment method which pulls on the parachute is an extractor parachute, which has been discussed in Section 1.2.2.1.

Moreover, engineers have modified and tailored these basic notions of deployment to the specific requirements of the mission. Other university teams have designed their own deployment mechanisms. An interesting approach is the Pneumatic Deployment System done by the Polish Team *AGH Space Systems* in 2018 for their *Turbulence* rocket, that developed their own ejection mechanism tailored for their double drogue chute recovery system with a 60 bar liquefied gas canister, shown in Figure 1.11.
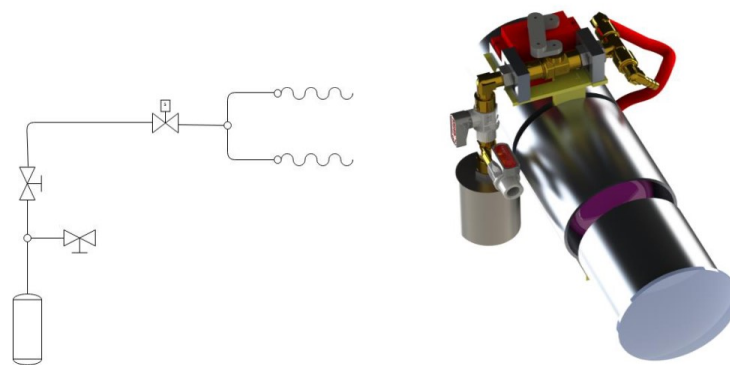
Figure 1.11: Double end Pneumatic Deployment System. Image provided by *AGH Space Systems*

Lastly, when as rockets quickly ascend into the atmosphere, the pressure differential between the interior of the recovery bay and the exterior becomes significant. This higher pressure on the inside may prematurely push the nosecone or other separable compartments. It is a common practice for engineers to drill small vent holes in the fuselage to allow pressure relief. When using hot gas or cold gas ejection to over-pressure the entire compartment area, said compartment must be pressurized

to the atmosphere and vent holes are not possible. In this case, engineers can opt for pressuring a smaller volume piston to push the content out of the rocket while implementing vent holes in the fuselage, at the cost of adding extra weight due to the piston mechanism. If, however, the pressure differential is not critical, a common solution is to locate *shear pins*. These small elements typically consist of nylon screws and are readily available in any *HPR* platform. They are drilled between the walls of the two separable compartments, holding them in place. At deployment, the over-pressure is enough to shear break these pins and allow for partition of the fuselage.

1.4.1   Line Sequencing

The order in which the different lines and components that make up the recovery system are progressively separated from the housing area is important. The distinct mass distribution, along with the generated drag forces and material elasticity, determine the behaviour and forces that deal with the re-acceleration of the masses to the speed of the falling rocket. This high-onset force is referred to as the *snatch force*, further discussed in Section 2.2. Figure 1.12 shows the three main sequencing mechanism for parachute deployment.
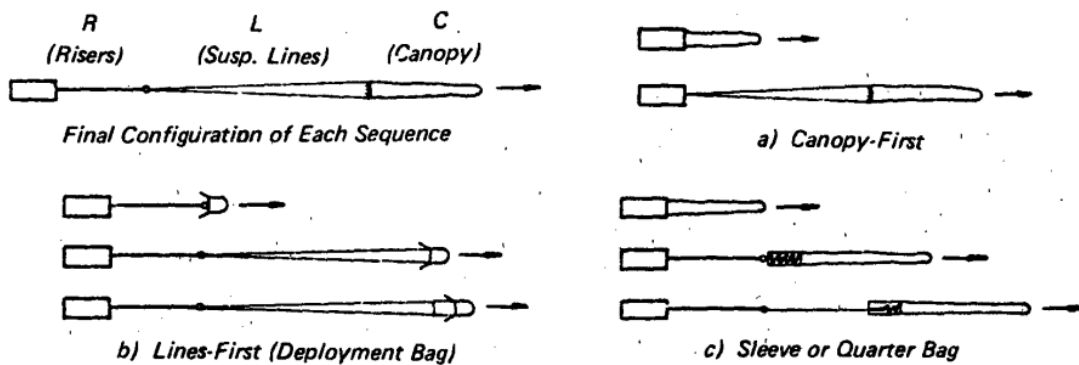
Figure 1.12: Parachute Sequencing Mechanisms [2]

1.5   Weight and Volume Estimation

Early recovery weight and volume estimations are very important in the first stages of development. These values are directly influenced by the loads the system will sustain during the mission and the allowed packing density the parachute system. Even though every recovery system has its own unique definitions and characteristics, the trend shows that percentage recovery weight decreases with the the total mass of the vehicle [3]. For *HPR* builds, Recovery System usually takes between 8% to 20% of the total rocket mass.

Loading is directly affected by the dynamic pressure during deployment and vehicle weight, discussed in Section 2.3.1. This loading affects the material selection and sequencing of the mechanism. If forces become too high, additional retarding stages may be considered, which may or may not increase the recovery weight and will require careful study and consideration. Kevlar is a desired material for shock cords

due to its much higher specific strength compared to nylon, significantly reducing weight. However, full kevlar systems are almost never used as the lower elasticity can cause substantial peak loading during deployment. Therefore, recovery lines are usually made up of a combination of these two materials. Some builds will even utilize a hybrid nylon-kevlar parachute to lower the mass of the mechanism up to 40% [3].

In order to lower the volume of the parachute assembly, larger rockets use mechanical or hydraulic pressure packing, combined with vacuuming the holding bag. However, depending on material selection, there is a maximum pressure packing value that, if surpassed, may damage and prevent correct deployment and inflation. Furthermore, engineers must be wary of not bending or breaking small metal elements such as reefing rings during this procedure, that may even gash the fragile canopy cloth.

Chapter 2

Aerodynamics and Modelling of Parachute Recovery

2.1 Recovery System Stability

Parachute body systems deal with both dynamic and static stability. A falling rocket may oscillate $\pm$ 5° which would technically render the set-up statically unstable. However, this same system is sufficiently dampened in the dynamic mode that it would be considered stable. As a result, every mission will have different stabilization requirements and will therefore use distinct parachute configuration. This damping effect that limits the oscillation amplitude and negates the effects of crosswind and other destabilizing phenomena such as Karman Vortex Trails is represented by the Stabilizing Moment Coefficient $\frac{\partial C_m}{\partial \alpha}$. If this term is negative, the amplitude of the oscillations diminish with time. The magnitude of this parameter determines the influence of this dampening effect. Appendix C elaborates on the stabilizing moment and angle of attack relationship.

Stability is also strongly influenced by the anchor point(s) of the parachute to the rocket. Single riser systems are inherently more unstable than multiple point linking. Even Geodetic Suspension line configurations have been developed for instances where stabilization was essential. However, these mechanism add complexity to the system. Thus, a compromise between rate of descent, stability, cost, weight, volume and complexity must be reached by Recovery Engineers.

(a) Non-Porous Canopy Airflow

(b) Porous Canopy Airflow

(c) Canopy with separation edge Airflow
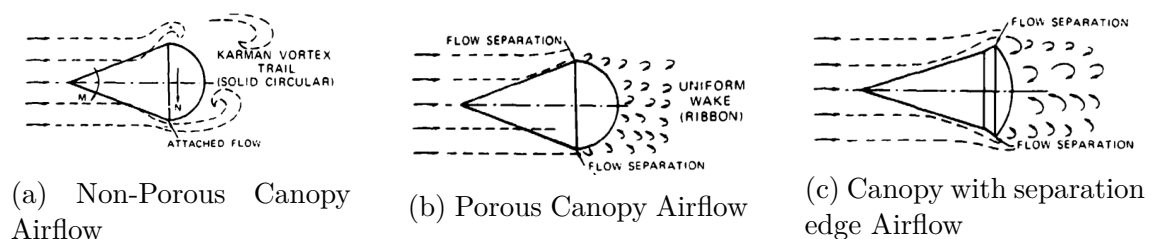
Figure 2.1: Airflow around non-porous, porous and separation edge parachutes [3]

2.2   Snatch Force

When deployment comes about, there is a time delay between initial separation and parachute line stretching. When the recovery lines are finally stretched while the rocket has been falling, the sudden re-acceleration of the recovery system mass generates a sharp transient force peak known as the *Snatch Force*. Following this short load, the parachute inflates, increasing the drag force leading to an *Opening Force*, discussed in Section 2.3. If the recovery system has been properly designed, this *Snatch Force* should not exceed the *Opening Force* in magnitude. Parachute bags allow a controlled slower unfurl of the parachute, minimizing the sudden jerk on the system.
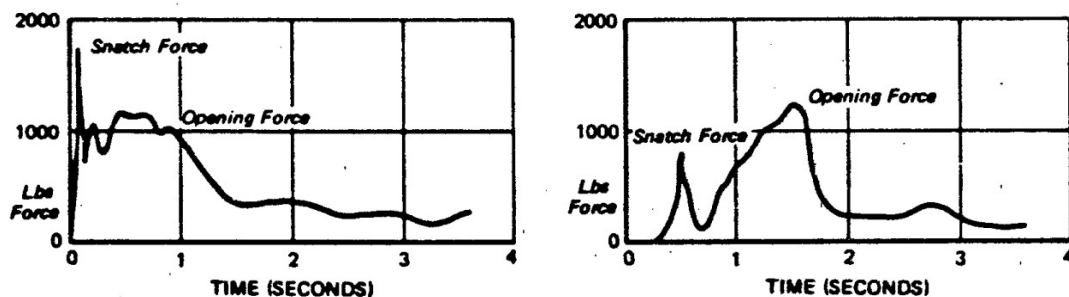
Figure 2.2: Effect of Deployment Bag on Relative Magnitude of Snatch Force. Left side refers to a Canopy-First Without Deployment Bag. Right side refers to a Line-First With Deployment Bag [2]

However, extreme peak loading has been observed in systems with permanently attached pilot/drogue chutes to the Main Parachute Canopy. The added drag by the previous decelerator greatly increases the likelihood of sudden high-onset forces. Furthermore, if the bridle that pulls on the Main Parachute Bag is too long, the sudden re-acceleration of the second recovery stage can cause both high *Snatch Forces* and improper Main Chute deployment [2].

2.3   Opening Shock and Canopy Loading

The second more problematic load is the *Opening Force*, determined by the inflation process of the parachute canopy. This can be divided into two distinct cases: *Infinite Mass* and *Finite Mass Condition*. This first term refers to cases where velocity change during inflation has been negligible which greatly simplifies the equations that govern this process. First stage and/or high speed drogue chute deployment meet the criteria to be considered Infinite Mass. The latter case occurs when there is a measurable velocity decrease as seen in final descent stages.

The final stages of the inflation process are governed by measurable parameters such as cloth porosity, viscoelastic material properties, canopy and mouth shape, masses and dynamic pressure of the system. However, the beginning is mostly determined by less tangible processes which add a certain randomness to the system [2]. Thus, great effort has been placed in modelling this phase of the recovery stage, with the aim of better understanding the loads that are generated and how
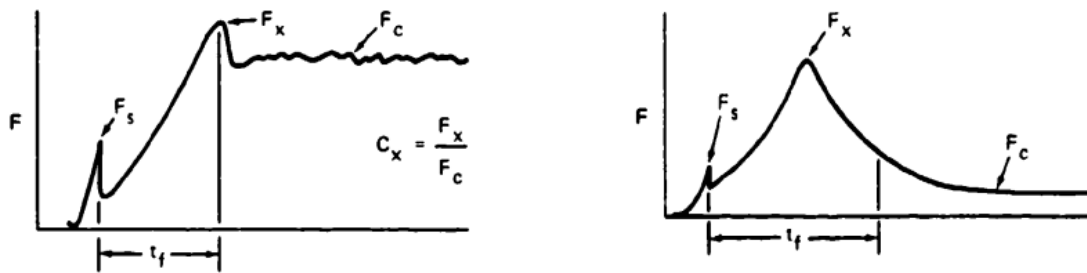
(a) Infinite Mass Inflation Force Profile

(b) Finite Mass Inflation Force Profile

Figure 2.3: Force Versus Time for Infinite and Finite Mass Conditions [3]

these can affect the integrity of the system. Due to the element of randomness, semi-empirical approaches have been developed to account for these so called drop-to-drop variations [13]. The following subsections provide and small theoretical overview of the different methods for Opening Force Calculation and their relevance. Detailed information on these procedures can be found in the respective Appendices.

2.3.1 Inflation Time

Inflation time is the most critical parameter when modelling the Opening Force Factor. There exists several procedures to estimate this value, which is defined as the time it takes the canopy to first reach its full steady state projected area. This, therefore, does not include the subsequent over-inflation of the parachute due to the elastic behaviour of the cloth and momentum of engulfed air.
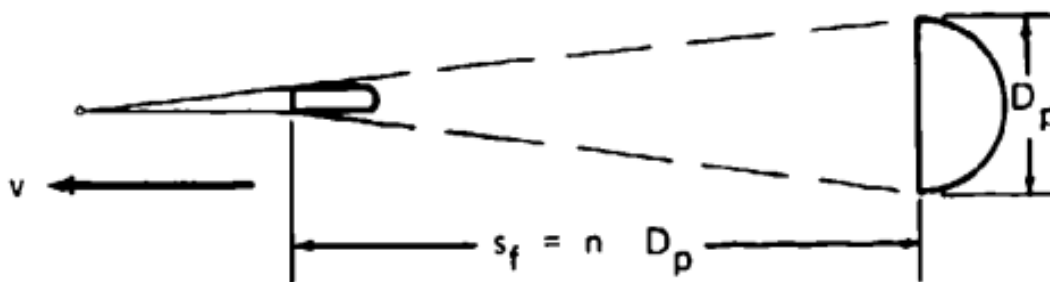
Figure 2.4: Filling Distance [3]

Experiments showcase the validity of the assumption that parachutes inflate in a fixed distance independently from the dynamic pressure [2][3][14]. This distance is set to be proportional to the nominal diameter D_0 of the parachute with the so called *canopy fill constant n*, which is tabulated for different parachute configurations. Attempts to fine-tune the basic Equation 2.1 for various parachute types can be found in [3]. Appendix F shows the tabulated values of n.

$$t_f = \frac{nD_0}{v} \tag{2.1}$$

Parachute Drag Area evolution and has also been investigated to estimate the transient behaviour of parachute inflation. Reference [9] indicates the common inflation curves for various parachute configurations. However, reference [15] attempts to solve the equations of mass conservation and Newton's Second Law for inflation time based on curve fitted data. This approach can later be used to numerically solve for inflation time (Equation 2.2 [1]) and parachute load evolution, which has been implemented in simple solvers like in Reference [16]. Appendix E expands on the theory behind this model for inflation time.

$$t_0 = \frac{14W}{g\rho V_s (SC_D)_0} \left[e^{\frac{g\rho \bar{V}_0}{2W} \left[\frac{(SC_D)_0}{A_{M_0} - A_{S_0} k \left(\frac{C_p \rho}{2} \right)^{\frac{1}{2}}} \right]} - 1 \right] \tag{2.2}$$

The parachute opening force formula is mathematically defined in reference [3] as:

$$F_x = (SC_D)_p q C_x X_1 \tag{2.3}$$

where:

- C_x = Opening Force Coefficient at Infinite Mass Condition. Value is found by wind tunnel testing, seen in Appendix G and depends on the parachute configuration. To be used in High Canopy loading conditions [3] as seen in Figure 1.3.

- X_1 = Force Reduction Factor - depends on the deployment conditions. Close to or equal to 1 for high speed drogue parachute deployment.

The product of these two parameters is referred to as the *Opening Force Factor* (C_k). As high speed drogue chute deployments have a Force Reduction Factor very close to 1, these two terms are sometimes loosely interchanged when dealing with Infinite Mass Conditions.

It has been found that there exists a noticeable relationship between the Opening Force Factor C_k and the so called *Mass Ratio* (R_m) [3][2][17][18][2]. This proves to be very helpful for obtaining fast estimates for parachute opening loads. This relationship is exemplified in Figure 2.5. The term $(SC_D)^{\frac{3}{2}}$ represents the volume of air engulfed by the inflated canopy. Thus, R_m is a measurement of the ratio of air collected by the parachute and the mass of the rocket.

$$R_m = \frac{\rho (SC_D)_p^{\frac{3}{2}}}{M_t} \tag{2.4}$$

---

[1]Original reference uses V_0 with a macron below to denote the Volume of air collected during inflation process. Here $\bar{V}_0$, with accent above, is used to avoid confusion

[2]Various papers define R_m as the inverse of the parameter given in this document.
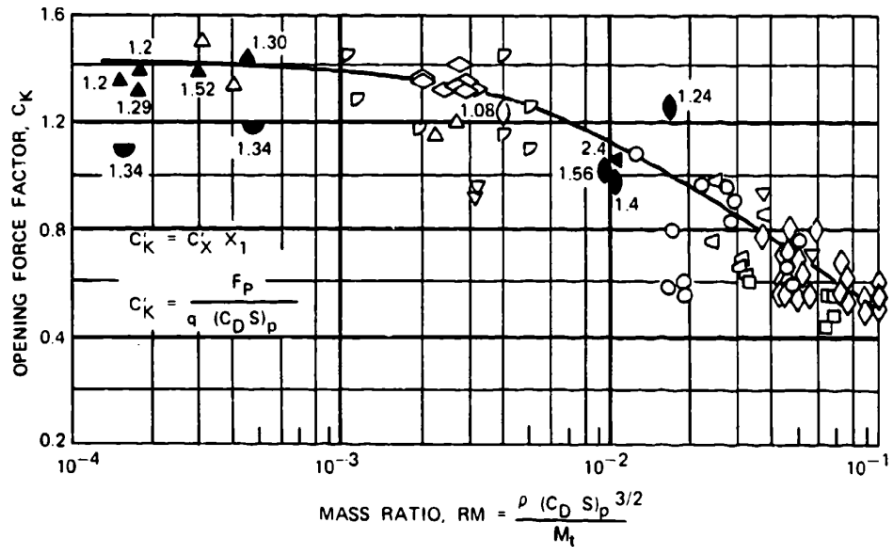
Figure 2.5: C_k - R_m Relationship [3]

2.3.2 Pflanz Method

This method allows for the estimation of the X_1 coefficient by means of curve fitted data from several drop tests. It shall only be used in accordance with the Infinite Mass Assumption. If it where to be used in Finite Mass Conditions, the yielded load will be larger. The X_1 dependency related to the dimensionless parameter A - *Ballistic Parameter* [3] is shown in Figure 2.6. The latter term relates the mass of air traversed during the inflation process and it is defined as:

$$A = \frac{2W_t}{(SC_D)_p \rho g v_1 t_f} \tag{2.5}$$

where:

- W_t = Total weight of the system.

- v_1 = Velocity at Line Stretch or start of disreef for intermediate stage calculation. This is **not** equal to the velocity at the beginning of deceleration/deployment (v_0). There will be some velocity decay that will affect the value of v_1.

- $(SC_D)_p$ = Drag Area of fully inflated profile or reefed configuration.

Engineers will choose the appropriate n value based on the parachute configuration, as seen in Appendix D. Coupled with the C_x value obtained from Appendix G, Equation 2.3 is solved for a Parachute Opening Force in Infinite Mass Conditions. This calculation can also be used for Finite Mass Conditions, whereby the overestimation of Peak Force serves as a safety factor.

---

[3]Reference [15] refers by Mass Ratio M to the Ballistic Parameter A shown in this document.
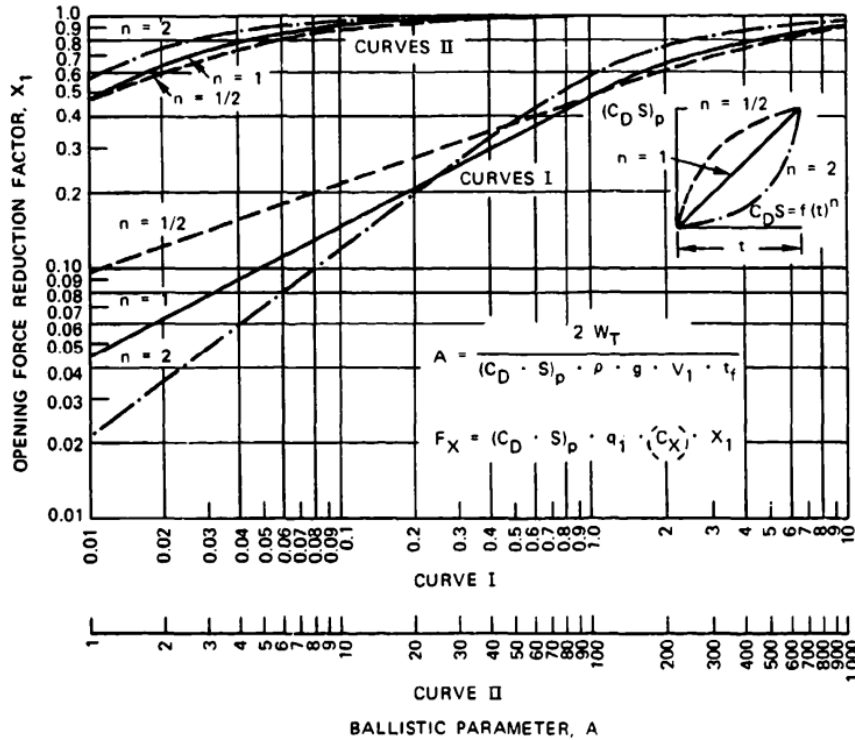
Figure 2.6: Opening Force Reduction Factor X_1 Versus Ballistic Parameter A

2.3.3 Ludtke Method

William Ludtke attempted to solve for an equation that would model the drag area evolution in inflating parachute canopies. He modified Equation 2.3 to the form:

$$F = (SC_D)_p q X_i \tag{2.6}$$

He uses curve fitted data to obtain an expression for X_i - *Instantaneous Shock Factor* in terms of the inflation time ratio $\frac{t}{t_0}$. This curve approximation is only valid for non-vented guide surface, elliptical, solid flat and 10% extended skirt parachutes, as they all exhibit similar drag area evolution [15]. He postulates that, for an initially closed parachute inlet ($\eta = 0$), X_i is:

$$\left(\frac{t}{t_0}\right)_{@X_{i_{MAX}}} = \left(\frac{21A}{4}\right)^{\frac{1}{7}}$$

$$x_{i_{MAX}} = \frac{16}{49}\left(\frac{21A}{4}\right)^{\frac{6}{7}} \tag{2.7}$$

This is also only valid for $A \leq \frac{4}{21}$ as for larger Ballistic Parameter [4] values, maximum shock force occurs later in the elastic phase of inflation ($t > t_0$). The procedure for higher A values is explained in Appendix E.

---

[4]Ludtke uses the letter M for the Ballistic Parameter A presented in this document, and names it *Mass Ratio*. To avoid confusion, Equation 2.7 is denoted with the nomenclature described beforehand.

2.3.4 Moment Impulse Theorem

The last method explored in this document to estimate the Parachute Opening Shock is based on the Moment-Impulse Theorem used to develop the *OSCalc - Opening Shock Calculator* [13][19]. Much like in Section 2.3.1, it expands on the $C_k - R_m$ dependency, relating the momentum change of a parachute system to the time integral of the external forces acting on said system. The process is elaborate and the details surrounding the methodology presented are beyond the scope and aims of this document. Appendix H showcases the calculation process of this case. Solving the momentum of the falling recovery system, an expression for the Opening Shock Factor is obtained (Equation 2.8).

$$C_k = \frac{2}{R_m n_{fill}^{gen}} \Gamma \tag{2.8}$$

This solution requires the computation of two integral-based terms. Educated guesses on the unknown parameters (namely I_F^{if} and Γ) based on previous experimental results allows for an estimate of C_k. As such, both an interpolated value of C_k and an analytical result may be used to estimate Opening Load.

- $n_{fill}^{gen} = \frac{V_i(t_f - t_i)}{(SC_D)_0^{\frac{1}{2}}} I_F^{if}$ is the generalized non-dimensional filling time. Used to distinguish between long and short inflation.

- $\Gamma = \frac{-(V_f - V_i) + \int_i^f g \cos\theta(t)dt}{V_i}$ is the non-dimensional term that encapsulates the net momentum change of the system.

Using *Matlab* software, the data on $C_k - R_m$ dependency used in [13] was interpolated from Reference [17]. A comparison between the two cases in shown in Figure 2.7. Long inflation corresponds to $n_{fill}^{gen} \geq 4$ and Short inflation to $1 \leq n_{fill}^{gen} < 4$.
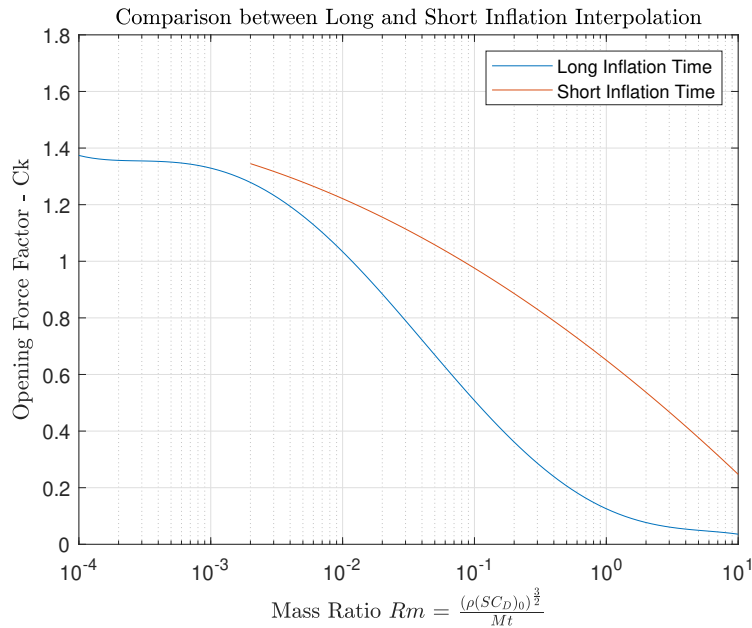
Figure 2.7: Comparison between long and short inflation time for interpolated $C_k - R_m$ dependency [17]

Chapter 3

Application for a Dual Deployment Sounding Rocket

3.1 Mission Description and Requirements

The theory behind the design of parachute recovery systems displayed in previous chapters is now applied to an own *HPR* build. The University Team, *Faraday Rocketry UPV* was accepted to compete at the 2022 edition of the European Rocketry Competition *EuRoC*, promoted by the *Portuguese Space Agency - Portugal Space*. The team will compete in the 3 km apogee solid motor boosted category with its *ASTRA* rocket. The relevant parachute recovery design constraints imposed by the competition are as follows [20]:

- Any launched body that exceeds an apogee of 450 m AGL must follow a *Dual Event* recovery. I.e. a descent profile in two distinct stages. This staging can be done by either main parachute reefing, previous drogue chute release or a combination of both.

- Independently recovered bodies, whose apogee is not anticipated to exceed 450 m are exempted from following two descent stages.

- Initial recovery must take place close or near apogee and shall result in a descent velocity of 23-46 m/s.

- Main Deployment event will take place at an altitude no higher than 450 m AGL and shall result in a terminal velocity of less than 9 m/s.

- Parachute assembly must be adequately shielded in the case of gas ejection deployment.

- Swivel links must be implemented to relieve torsion on parachute lines and prevent suspension line tangling.

- If separate parachutes are used, they should be visually dissimilar from each other and shall also contrast clearly with the blue sky and grey clouds.

3.1.1 Internal Design Constraints

The student team *Faraday Rocketry UPV* was founded in the beginning of summer 2021 and none of the 40+ members had any prior experience with rocketry. As such, low University funding, overall lack of previous knowledge and information availability play a key role in the design philosophy of the *ASTRA* project. A compromise between keeping the rocket design simple but also laying a solid foundation for the future development of larger more technologically advanced builds must be found.

This lack of experience and having only one year margin for the whole process meant that key recovery subsystems, such as the parachute itself, were bought from parachute manufacturers, instead of constructing a parachute tailored to our specific needs. This forces the design to be somewhat centered around commercially available technology. Furthermore, with the aim of gathering sponsorship for the team, obtaining materials from local or national industry was prioritised over foreign companies, even if the international solution better suits the rocket's design. Additionally, components bought outside of Spain more often than not need special treatment at customs, significantly increasing time delays and shipping costs, which is undesirable given the low budget and time constraint.

It must be stated that like any engineering project, the design of this sounding rocket is an iterative process. As a result, broader estimates are initially made to have an order of magnitude on which to work from. As the project advanced, on top of the aforementioned design constraints, the *Structures Department* fixed the recovery size and rocket weight to the following measurements:

- Interior Diameter: $\phi_0 = 90$ mm

- Recovery Bay Length: $L \in [350,550]$ mm

- Recovery Mass: $m_{rec} \in [0.75, 2]$ kg

- Rocket Dry-Mass[1] $m_{rocket_0} \in [10.5,12.5]$ kg

- Main Parachute Descent Rate: $v_f \leq 7$ m/s

3.2 Recovery and Ejection Method Selection

Before deciding which deployment method, as described in Table 1.3, will be implemented, limitations imposed be the Manufacturing and Structures Departments had to be taken into account. The fiberglass fuselage, reinforced with aluminum rings and steel bars in a semi-monocoque configuration was complicated enough for a first build that it was ruled that no large orifices were to be made to the fuselage. This meant that side deployment or any other non-axial deployment methods were ruled out. Larger sounding rockets, such as the Spanish PLD Space *Miura 1* rocket, house the recovery system near the rocket motor retainer. This way, they take advantage of this element's resistance to absorb the impact of the snatch and opening shock force of the parachute [11].

---

[1]In rocketry, unlike aviation, dry-mass refers to the Total Mass of the vehicle without the propellant.

Therefore, the deployment philosophy seen in Figure 1.7 is not possible in this project. Larger rockets do not separate their fuselage into three distinct structures due to scalability and stability issues. With the aim of acquiring experience in more advanced set-ups, it was decided to perform a single recovery bay deployment.

Regarding how the staging of the recovery is performed, the rocket could either use a drogue and main parachute and/or implement a reefing system on the main canopy. Reefing is a more elaborated system that is key in heavier rockets. However, based on the initial weight estimates for *ASTRA* (7-16 kg), reefing as a means of additional staging would only add unnecessary complexity to the system. Ultimately, based on the amount of information available regarding the use of drogue and main parachutes compared to reefing systems, it was decided early on that the previous method will be implemented. As a result, the recovery system was limited to using a drogue and main parachute, the latter stowed in a deployment bag.

Deployment System	Complexity	Max. Rocket Size	Weight	Reaction Load	Ejection Velocity
Hot Gas	1	1	1	2	3
Cold Gas	1-2	2-3	1-2	2	3
Spring	2	1	2	2-3	1-2
Mortar	4	5	5	5	4-5
Slug Gun	4	5	3-4	2-3	4-5
Tractor Rocket	4	5	2	1	4-5
Pilot Chute	1-2	5	2	1	1-5

Table 3.1: Modified Table 1.3 for Deployment Method Assessment. Green = Desirable. Yellow = Neutral. Red = Undesirable.

Finally, an ejection mechanism for the recovery system had to be evaluated. Table 1.3 is modified to better understand the design assessment. Pilot Chute deployment, although a valid solution in terms of complexity, is discarded due to *EuRoC*'s constraints. This is a form of aerodynamic extraction that requires the falling rocket to attain a certain dynamic pressure and speed to effectively pull on the system. As the competition rules state that deployment shall occur at or near apogee where velocity is minimal, this method is ruled out.

Only **Hot Gas**, **Cold Gas** and **Spring** ejection mechanisms remain a suitable solution for the task at hand. Several design iterations where considered for these systems.

3.2.1   Spring Ejection

Originally, *ASTRA* had an internal structure design where four aluminium profiles ran through the entire length of the rocket. Therefore, a spring loaded system with redundant servo activation placed in said profiles was proposed. The servo would apply a small torque that would be enough to turn the latch mechanism holding the spring, seen in Figure 3.1. The system had to be able to counteract the holding force of the shear pins, as explained at the end of section 1.4, and have enough remaining strength to eject the recovery system. With this system, the team intended to bring a new design to the table, as no other redundant spring loaded mechanism had been used for recovery ejection.

(a) Overview

(b) Open Latch

(c) Closed Latch
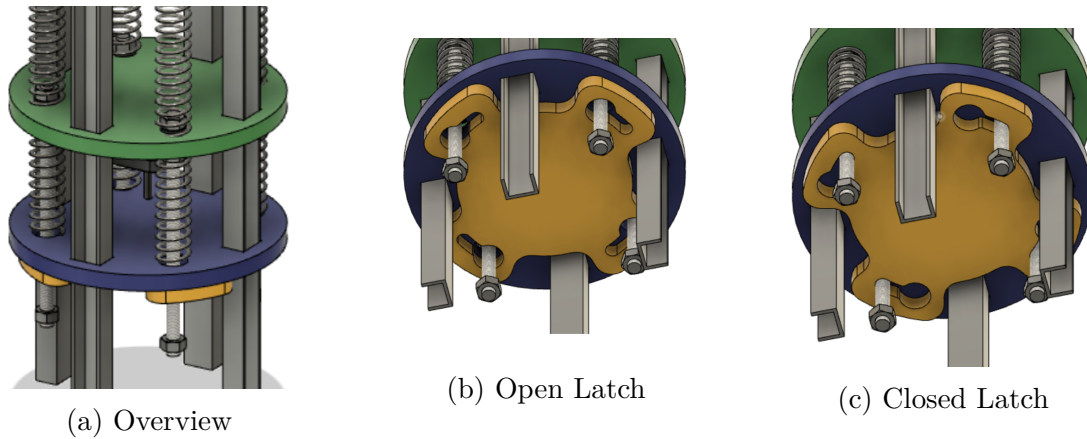
Figure 3.1: Final Spring Ejection System Iteration. CAD modeled in *Fusion 360*.

Worst case scenario had to be considered for the shear pin retention force. The fixed 90 mm interior diameter of the rocket meant that if for any reason no venting occurred during ascension, the pressure differential inside the recovery area would be around $\Delta p = 31200 Pa$, which amounts to an inside outwards force of around 200 N [2].

$$F_{spring} = k\Delta x \tag{3.1}$$

The Spring Force had to be sufficient to accelerate the recovery and nosecone mass with enough velocity to allow proper drogue parachute inflation. However, the volume constraint of the recovery base meant that high spring constant springs had to be used. Equation 3.1 illustrates this problem. A compromise between an adequately high Spring Constant k value and mechanism that allowed high spring compression to allow enough room within the fuselage to house the recovery system was deemed too complicated to implement. These high compression forces also meant that mounting the system would become a potential pinching hazard. Due to the complexity, low volume efficiency, high weight and mounting hazard, this deployment method was discarded.

3.2.2 Cold Gas Ejection

The original internal structure design was abandoned by the Structures Department. The relatively small recovery housing volume meant that deployment by cold gas over-pressure was possible. However, due to the low budget constraint, commercial CO_2 systems, seen in Figure 1.10, were not an option. Instead of pressurizing the whole recovery area, it was first decided to attempt to fill a smaller pneumatic piston, much like the system seen in Figure 1.11. This meant that bigger venting holes could be implemented, which significantly lowered the risk of premature nosecone separation due to pressure differential.

Here, a small readily available CO_2 canister would be opened by a small pyro activated punch and quickly fill the piston, ejecting the recovery system. However,

---

[2]ISA +0 model was used for this calculation based on the launch area in Ponte de Sor and time of the year (October).

Figure 3.2: Considered Pneumatic Piston from Festo$^{©}$

the considered pneumatic pistons from *Festo $^{©}$* that fitted the size and weight constraints were capped at 10 bars around 150 psi of operating pressure, with 15 bars or 220 psi of maximum allowed inside pressure [21]. CO_2 cartridges are housed at 20ºC at around 58 bars or 850 psi of pressure [22].

This leads to an initial peak pressure inside the piston too high for the system to work properly. Either small over-pressure valves would need to be mounted or risk damaging several pistons due to over-pressure issues. These technical issues rendered the cold gas piston system obsolete. A cold gas ejection mechanism with no pneumatic piston still remains a valid solution for the task at hand. Nevertheless, the low time constraint and overall availability and simplicity of the black powder ejection mechanism led to the decision to develop the cold gas ejection for future larger builds.

3.2.3 Black Powder Ejection

The main drawbacks of Black Powder Ejection, as mentioned in Section 1.4, are the low scalability of the mechanism, potential harm to the parachute cloth and difficulty of black powder size estimation. To counteract this issue, the same piston mechanism as in Section 3.2.2 could be activated by a small calculated black powder charge, much like the British University Team *Leedsrocketry* did for their rocket in the 2022 edition of the *Spaceport America Cup*. However, budget and time constraint limited the ejection system to be performed with the basic methodology of black powder ejection, where the whole recovery bay is pressurized.

$$pV = mRT$$

$$m_{BP}[kg] = \frac{p[Pa] \cdot V[m^3]}{119.24 \left[\frac{J}{kgK}\right] \cdot 1837[K]} \tag{3.2}$$

Approximations for preliminary black powder mass needed for successful deployment may be employed [23][24], based on the *Ideal Gas Law Equation* as seen in Equation 3.2. However, experience during the construction of the *ASTRA* project has shown that these are very broad estimates and vary greatly depending on the burn rate and grain quality. Rather, engineers should perform several tests to fine-tune the

(a) Test Bulkhead with BP charge   (b) Mounted BP charge
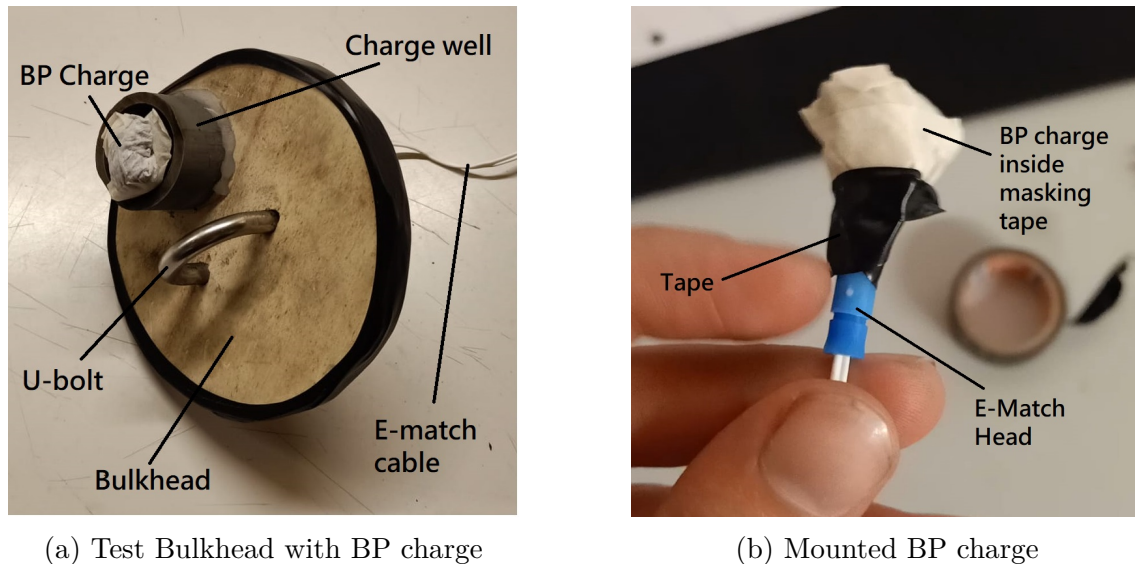
Figure 3.3: Black powder charge mounted on test bulkhead

amount needed, which for this project is explained in Section 4.1.1.1. In essence, an electronic match is encapsulated with a black powder charge and sealed in a tightly folded paper or plastic sheet. This charge is typically rested on a small charge well on the recovery bulkhead, as seen in Figure 3.3a. The bulkhead has a small hole in the middle of the charge well to allow the electronic match cable to connect to the Avionics bay located below.

As a starting point, a net pressure acting on the interior of the nosecone of 103.4 kPa (1.034 bar or 15 psi) is desired to eject the recovery system. Given the initial recovery bay area length constraint of $L \in [350,550]$ mm, shown at the end of Section 3.1.1, the initial black powder charge size estimation amounts to a range between 1 and 1.65 grams. Section 4.1.1.1 showcases the test results to determine the best black powder amount needed.

3.3   Parachute Selection and Loading

Once the ejection method has been established, the next critical component that directly affects the design of the system is the Parachute Selection and forces generated during deployment. As mentioned in Section 3.1, the lack of time and experience meant that parachutes could not be specifically designed for this rocket. Instead, commercial systems had to be assessed until the best option was found. It will then later be tested to ensure calculations were correctly performed, as described Sections 3.3.1 and 3.3.2. Furthermore, due to the lack of experience and time, cluster configurations had to be avoided.

Commercial Parachutes that were able to achieve the desired terminal velocity were assessed and selected based primarily on cost, weight and material selection. It must be stated that the atmospheric density varies with altitude. In this project, the $ISA + 0$ model is used [25]. As a result, acceptable parachutes had to reach the correct terminal velocity within their given altitude range and weight estimate of the rocket. As for the parachute opening forces, the scarcity of available parachutes

forced the team to first select a specific parachute and then size the rocket's recovery anchor point for that specific element.

$$F = ma = 0 = Weight_{rocket} - Drag_{parachute} - Drag_{rocket}$$

$$m_0 g = \frac{1}{2} \rho[z] v_{final}^2 \left[(SC_D)_r + (SC_D)_0 \right]$$

$$v_{final} = \sqrt{\frac{2 m_0 g}{\rho[z] \left[(SC_D)_r + (SC_D)_0 \right]}}$$

(3.3)

Steady State Descent Velocity can be calculated by solving Newton's second law of motion. The drag coefficient of the rocket (C_{D_r}) is assumed to be around 0.75 coupled with its cross-sectional area, based of the Structures Department's simulations. As the exterior diameter of the rocket is fixed to $\phi_{ext} =$94 mm, the term $(SC_D)_r$ is directly computed. With the $ISA + 0$ model for atmospheric density, a graph of terminal velocity against altitude is obtained. The terrain elevation of the expected drop site is needed to know the height interval in which the parachute will be deployed. This is, to ensure the terminal velocity never exceeds the self-imposed limit of 7 m/s. The *EuRoC* launch site is located in *Campo Militar de Santa Margarida*. Figure 3.4 shows that terrain height varies between 50 and 200 meters. As the main parachute will be deployed no sooner than at 450 m AGL, the z range for atmospheric density in this phase will be between 50 and 750 m. For the drogue chute deployment, the z range will be 500 and 3200 m.
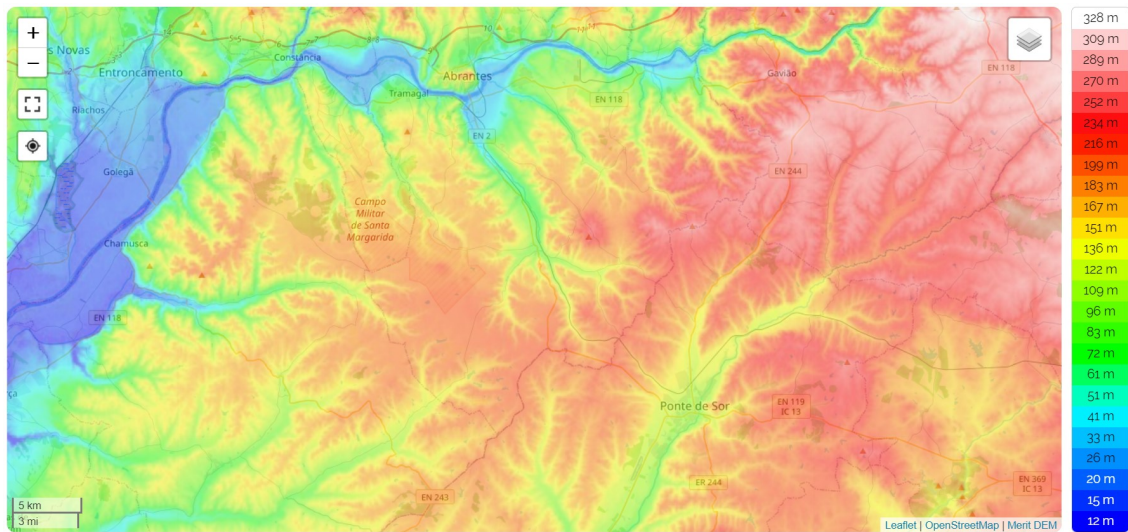
Figure 3.4: *EuRoC* launch site terrain elevation [26]

3.3.1 Drogue Chute Selection

As explained in Section 2.3, the Opening Shock Force exerted during deployment is directly proportional to the dynamic pressure of the falling parachute system. In the case of this project, as drogue deployment occurs close to apogee where speed in lowest, the opening force of this first parachute will be lower than that of the Main Parachute. As such, the limiting factor in this case for sizing the recovery system anchor is the Main Parachute Opening Force. Therefore, even though drift

distance would be increased, it is desired to use a Drogue Parachute that will drop the rocket closer to the lower bound of *EuRoC*'s cosntraint of 23 m/s. A self-imposed new upper limit for the rate of descent of 35 m/s is also considered. Compatible Parachutes Descent Profiles are shown in Figure 3.5.
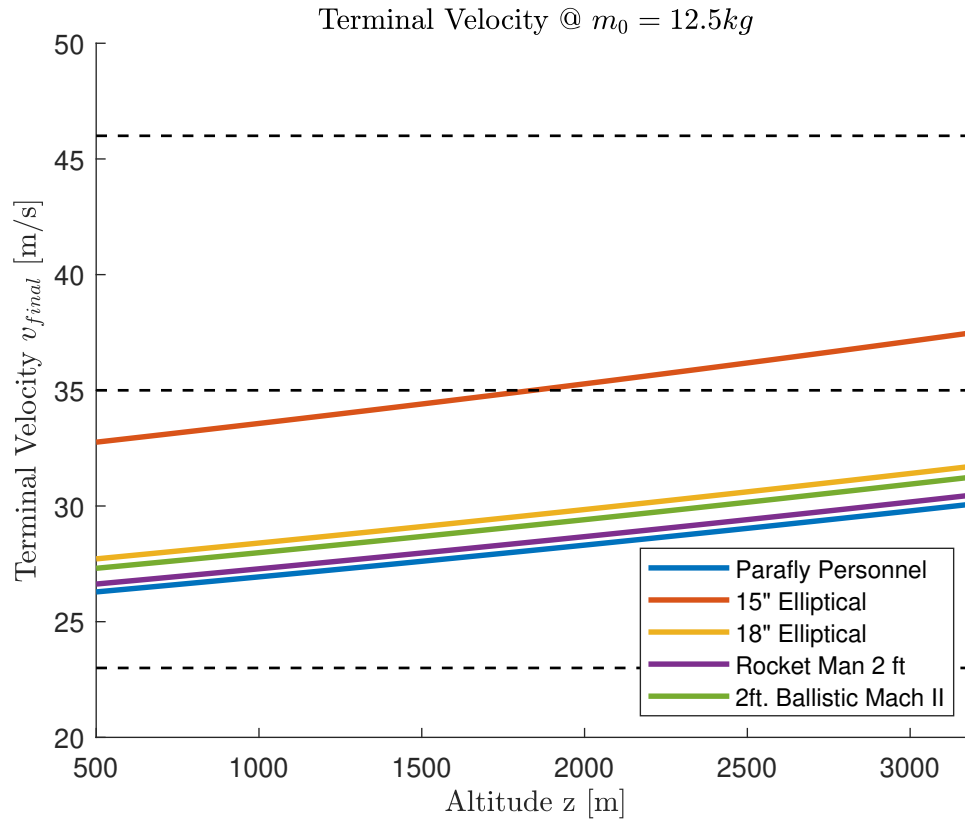
Figure 3.5: Drogue Parachute Terminal Velocity Graph for various compatible parachutes.

Table 3.2 shows the properties of the parachutes and whether they are beneficial towards the recovery system's design [3]. Sponsorship from the National Military Grade Parachute Manufacturer *Parafly, S.A* allowed for a suitable decelerator to be used for free. Even though this parachute, seen in Figure 3.6, is designed for personnel stabilization in army maneuvers, it remains more than a valid option for this project. The mass of the parachute includes the 1 m long nylon sling attached to the confluence point. A net is sewn instead of traditional suspension lines to prevent inversion of the parachute.

Name	Type	Mass [g]	Packing volume [cm3]	SCD	Final Velocity [m/s]	Cost [EUR]
Parafly Personnel	Solid Flat Circular	102	210	0.285	26.3	Free
15" Elliptical	Elliptical	43	135	0.177	32.8	120
18" Elliptical	Elliptical	60	160	0.255	27.7	120
Rocket Man 2 ft	Square	42	130	0.277	26.6	60
2ft. Ballistic Mach II	Square-Cross	170	1030	0.262	27.3	110

Table 3.2: Drogue Parachute Comparative Rating Table. Green = Desirable. Yellow = Neutral. Red = Undesirable.

---

[3]Prices for parachutes have been estimated based the cost stipulated on their respective websites and on prior experience with customs and mailing companies.

Ideally, the same Opening Force Estimation would be made for various parachutes and contribute in the decision making process for parachute selection. In this case, as the limiting factor is the Main Parachute Force, this estimate will only influence the mechanical requirements of the Drogue Chute lines. Additionally, due to the sponsorship, only *Parafly*'s option is ultimately considered and its load evaluated for line sizing. The details and working out of the following values shown in Table 3.3 is explored in Appendix H.

(a) Hanging Profile   (b) Inflated Profile
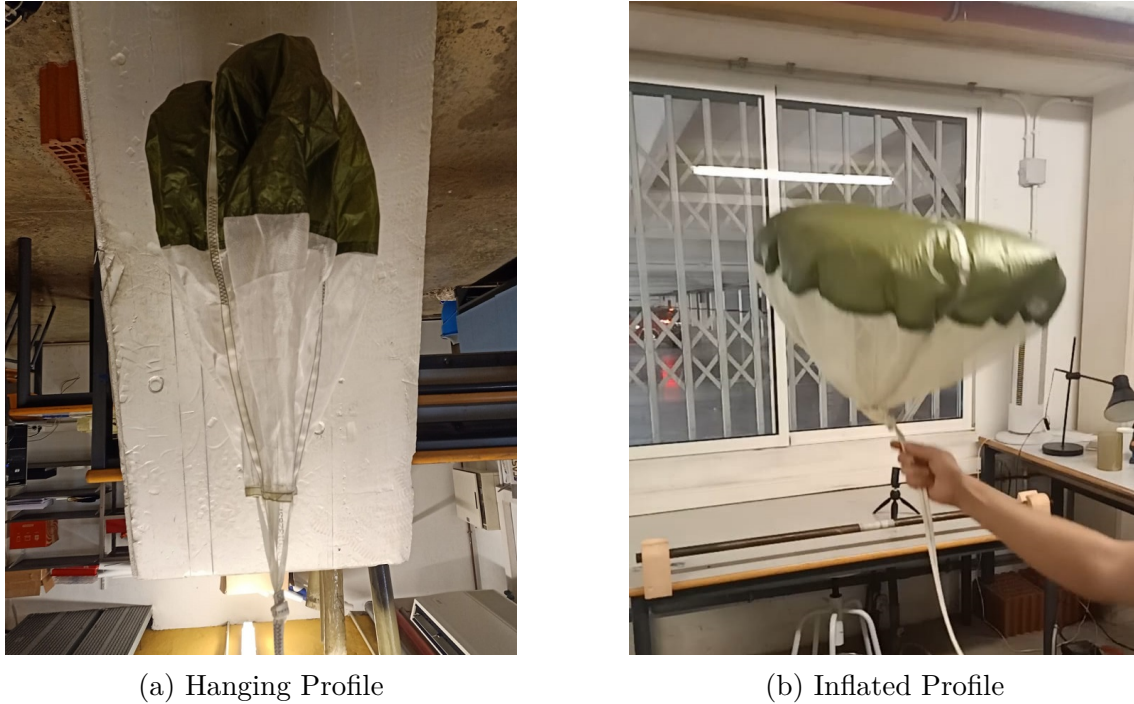
Figure 3.6: *Parafly*'s Drogue Parachute

Due to overall inexperience when dealing with parachute recovery systems, the highest estimated opening load is considered for the sizing of the drogue lines. Larger rockets will employ more advanced simulations such as *Monte Carlo* simulations and then obtain a Safe Operating Range. In this project, however, a worst case scenario where a higher than expected velocity is considered for the Force Estimation, as an additional Safety Factor. For the Drogue Deployment, a velocity at line stretch (v_{ls}) of 80 m/s is considered, which amounts to a free fall of around 8 seconds past apogee, assuming a near complete vertical flight path. Furthermore, even though Appendix F shows the filling time constants (n) for various parachutes, a conservative value of 4 is used. This is done under the assumption that smaller and lighter parachutes inflate quicker that their larger counterpart, even though they are of the same configuration. This reduces the filling time, which in turn increases the opening force.

An attempt to analytically approximate the Ck value following the Moment Impulse Theorem method is made. However, these are highly susceptible to drop-to-drop variations which, as explained in Section 2.3.4 and Appendix H, are accounted for using an upper and lower bound in the interpolation. Lastly, as seen in Appendix G, an Infinite Mass C_x value of 1.7 is used for the Pflanz Method described in Section 2.3.2.

- $\rho = 0.909 \text{ kgm}^{-3}$
- $q = 2909 \text{ Pa}$
- $D_0 = 0.72 \text{ m}$
- $v_i = 80 \text{ m/s}$
- $m_0 = 12.5 \text{ kg}$
- $C_{D_0} = 0.7$

Deployment Characteristics			
Ballistic Paremeter - A	33.5		
Mass Ratio - M_r	0.011		
t_f (Knacke) [s]	0.036		
t_0 (Ludtke) [s]	A		
Moment Impulse Theorem			
Ck - avg	1.21	Fmax [N]	1005
Ck - upper	1.58	Fmax [N]	1306
Ck - lower	0.85	Fmax [N]	703
Pflanz Method			
X_1	1	Fmax [N]	1409
Ludtke Method			
X_1	1.45	Fmax [N]	1205

Table 3.3: Opening Force Estimation for Drogue Parachute.

As the Opening Force Reduction Factor X_1 is equal to 1, a complete Infinite Mass condition is met. Therefore, Pflanz Method yields the highest Load. This value, highlighted in red, is used to determine the necessary strength for the Drogue Parachute Lines.

3.3.2 Main Parachute Selection

As with the Drogue Parachute, several viable options are plotted in Figure 3.7. Only *Rocketman*'s 9 ft square parachute and *Fruity Chute*'s IFC Iris Ultra Standard - 72" toroidal parachute can confidently lower the rocket with a dry mass of 12.5 kg below the 7 m/s limit. It may very well be that the final dry mass of the *ASTRA* rocket is lower than 12.5 kg and therefore, the other two parachutes shown in the graph would also comply with the imposed Recovery Requirements, lowering the cost. However, the terminal velocity being lower than 7 m/s was an immovable condition by the Structures Department. In the unfortunate case that the rocket's dry mass increased later in development or that the parachutes underperformed, the team decided to play it safe and consider only the former two decelerators.

It is expected for the Main Parachute to begin inflation at a slightly higher velocity than the Drogue Chute final descent rate at the designated altitude, in this case being 27 m/s. This increase is due to the stage separation procedure, where rocket and drogue parachute separate from one another and begin a very short freefall until the deployment bag is completely pulled and deployed. However, as an additional security factor, a higher than expected terminal velocity of 40 m/s is used for the Force Estimation. Finally, even though Pflanz Method, as explained in Section 2.3.2, can only be used under Infinite Mass Conditions [3], it is still shown in Tables 3.4 and 3.5 for comparative reasons. The Details of the calculation can be found in Appendix H.
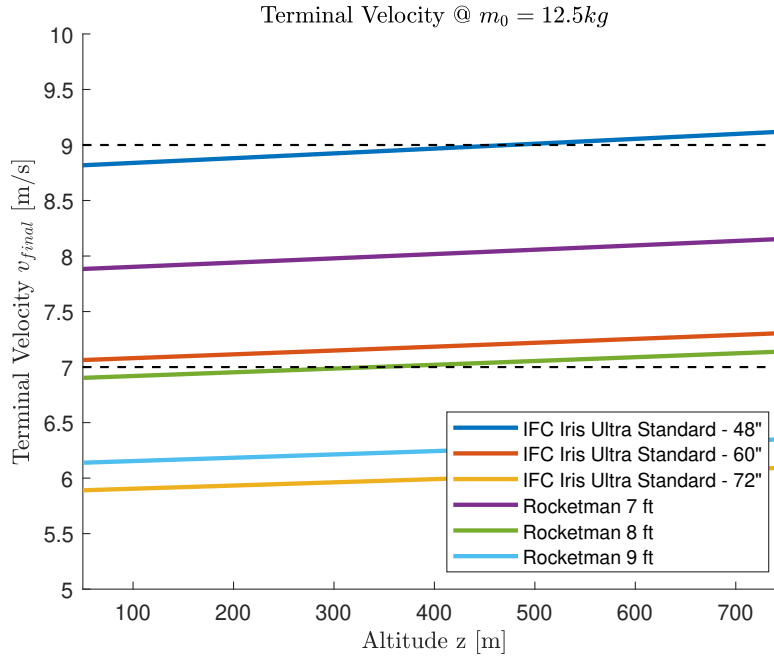
Figure 3.7: Main Parachute Terminal Velocity for various compatible parachutes.

The deployment conditions of the Main Parachute are the following:

- $\rho = 1.165$ kgm^{-3}
- $v_i = 40$ m/s

- $q = 932$ Pa
- $m_0 = 12.5$ kg

Fruity Chutes IFC 72" Parachute [4]

- $D_p = 1.83$ m
- $D_0 = 2.36$ m
- $C_{D_0} = 1.32$

Deployment Characteristics			
Ballistic Paremeter - A	0.394		
Mass Ratio - Mr	1.29		
tf (Knacke) [s]	0.236		
t0 (Ludtke) [s]	A		
Moment Impulse Theorem			
Ck - avg	0.609	Fmax [N]	3278
Ck - upper	0.792	Fmax [N]	4261
Ck - lower	0.426	Fmax [N]	2295
Pflanz Method			
X1	0.352	Fmax [N]	3219
Ludtke Method			
X1	[-]	Fmax [N]	[-]

Table 3.4: Opening Force Estimation for IFC 72" Main Parachute.

---

[4]Fruity Chutes categorizes their parachutes by their projected diameter. For the sake of consistency, the Nominal Diameter D_0 is calculated based on the Total Parachute Area

Rocketman 9 ft Parachute

- $D_0 = 2.74$ m
- $C_{D_0} = 0.9$

Deployment Characteristics			
Ballistic Paremeter - A	0.368		
Mass Ratio - Mr	1.14		
tf (Knacke) [s]	0.274		
t0 (Ludtke) [s]	A		
Moment Impulse Theorem			
Ck - avg	0.629	Fmax [N]	3118
Ck - upper	0.818	Fmax [N]	4053
Ck - lower	0.440	Fmax [N]	2182
Pflanz Method			
X1	0.343	Fmax [N]	2895
Ludtke Method			
X1	[-]	Fmax [N]	[-]

Table 3.5: Opening Force Estimation for Rocketman 9 ft Main Parachute.

Both parachutes exhibit very similar results and both are suitable candidates for this project. Ultimately, due to advisor recommendations, *Fruity Chute*'s IFC Iris Ultra Standard 72" Parachute is employed. Furthermore, the same company offers a deployment bag compatible with the dimensions of the *ASTRA* rocket. Its characteristics are listed below in Table 3.6.

Cd0	1.32	Mass [g]	380
D0 [m]	2.36	Packing density [cm^3]	1215
S0 [m^2]	4.37	Type	toroidal
Dp [m]	1.83	Cost + shipment [EUR]	$\approx$ 380

Table 3.6: *Fruity Chute*'s IFC Iris Ultra Standard 72" Parachute Parameters

3.4 Lines Diagram and Elements

The lines diagram showcases how all the elements and mechanisms are organized in the recovery system. A simple design that fits the design requirements explained in Section 3.1 and is compatible with the Hot Gas - Black Powder ejection mechanism shown in Section 3.2.3 must be found. Furthermore, it is desired to include redundant mechanism when possible. The size and mechanical properties of the elements used are determined based on the Snatch and Opening Force of the Parachute explained in Sections 3.3.1 and 3.3.2. After several iterations, the final design shown in Figure 3.8 was found.
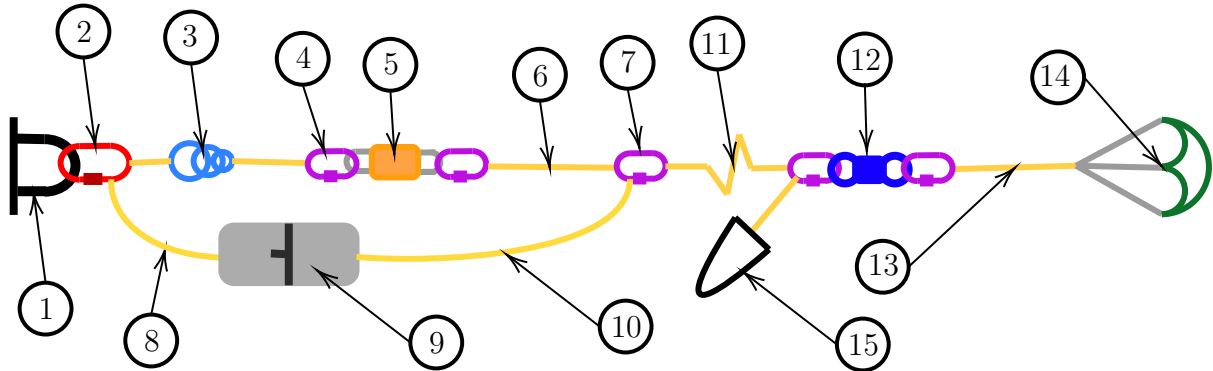
Figure 3.8: *ASTRA* Lines Diagram

- **1:** U-bolt
- **2:** ϕ 8 mm Quicklink
- **3:** Triple Ring Release
- **4:** ϕ 5 mm Quicklink
- **5:** L2 Tender Descender
- **6:** Drogue Release Bridle
- **6:** Grouping Quicklink
- **8:** Main Riser Cord

- **9:** Main Parachute D-Bag
- **10:** D-Bag Opening Bridle
- **11:** Drogue Riser Cord
- **12:** ϕ 5 mm Swivel
- **13:** Drogue Nylon Riser
- **14:** Drogue Parachute
- **15:** Nose cone

The deployment mechanism will pressurize the recovery area and push the Drogue Parachute (13) far enough for proper inflation to occur. The drogue will pull any remaining cords until the whole Drogue Line is taught. This sudden tension in the lines is what was referred to as *Snatch Force*, as seen in Section 2.2. The Drogue Chute lines are composed of elements (2) to (6) and (10) to (13). Elements (2) to (9) are still found withing the rocket's fuselage during descent, whereas elements (10) to (13) are under the influence of the surrounding airflow. The U-bolt (1) seen in at the left side of Figure 3.8 is attached to the bulkhead located just below the recovery bay area. This is the anchor point of all the recovery components to the rest of the rocket. The larger Quicklink (2), connects all these lines to this u-bolt (1). These two elements are seen in Figure 3.9.

Figure 3.9: U-bolt and Quicklink

Once the Main Parachute Deployment Condition has been met, both the Triple Ring Release (3) and Tender Descender (5) will activate. For redundancy purpose, they have been placed in series and will only take the activation of one of these components to 'cut' the Drogue Parachute Lines. In order for no objects to be ejected out the rocket and freefall to the ground, small cords are placed to secure this elements to the rocket. To not complicated the diagram, they have been omitted. The different principle of action also adds to the redundancy and security of the system. When this event happens, bridle (9) is still slack due to the difference in length. Figure 3.10 shows this sequencing.
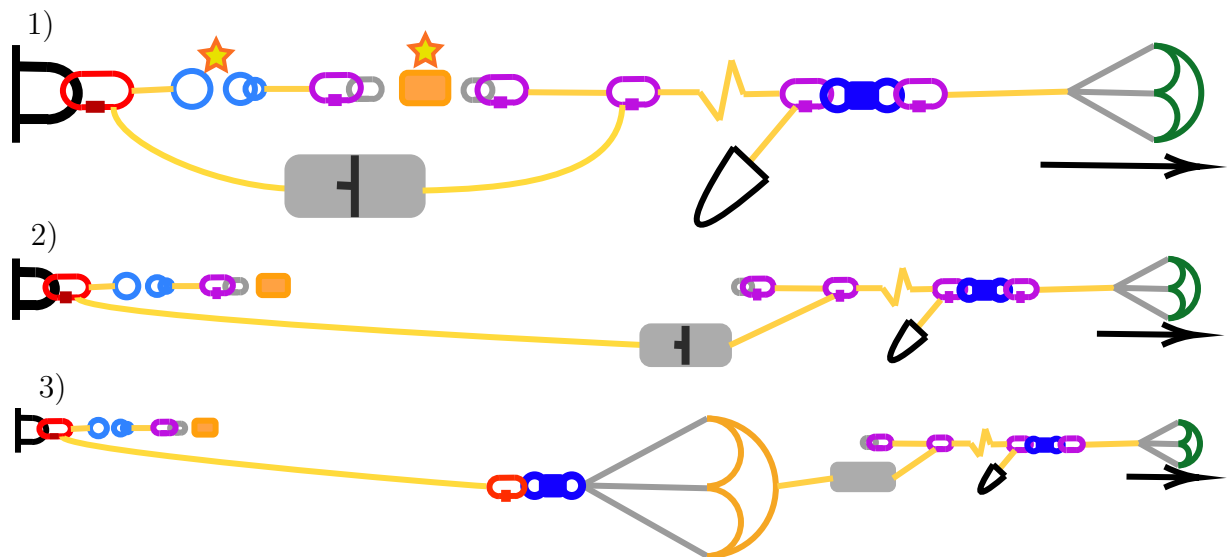
Figure 3.10: *ASTRA* Main Chute Deployment Sequencing

Both the rocket and the Drogue Parachute begin to freefall and their trajectory can be derived from Newton's Second Law. As this event will happen in a relatively short window of altitude, density can be considered constant to simplify the calculations. Equation 3.4 shows the relationship between the forces acting on both the Upper Drogue Parachute System, comprised in this case by elements (6), (7) and (11) to (15), and the mass of the rest of the rocket. A sufficiently large velocity difference is desired to pull on the main bag through the opening bridle (10) with enough tug

that the Main Riser Cord (8) is effectively pulled out of the Deployment Bag (9). Once the whole riser has been pulled (event 2 to 3 in Figure 3.10), the same bridle will fully open the deployment bag housing the main parachute. The deployment bag is also attached to the apex of the parachute. This way, the previous drogue system will not separate from the rest of the rocket, as it is a condition imposed by *EuRoC*'s guidelines.

$$
\begin{aligned}
m_p \ddot{x}_p &= m_p g - \frac{1}{2} \rho \dot{x}_p^2 \left[(SC_D)_0 \right] \\
m_r \ddot{x}_r &= m_r g - \frac{1}{2} \rho \dot{x}_r^2 \left[(SC_D)_r \right] \\
\dot{x}_p(0) &= \dot{x}_r(0) \approx 27[m/s] \\
x_p(0) &= x_r(0) = 0[m]
\end{aligned} \tag{3.4}
$$

However, excess slack in both the opening bridle (10) and the bridle connecting the deployment bag to main parachute apex can cause increased Snatch Forces that may damage the parachute system [2]. Therefore, a compromise must be met. Solving the system of Equations 3.4, a graph of relative speed $\dot{x}_p = \dot{x}_r$ against relative distance $x_p = x_r$ is plotted. This way, a sensible bridle length is found. A final length of 1 m difference, corresponding to a pull velocity of around 20 m/s is chosen.
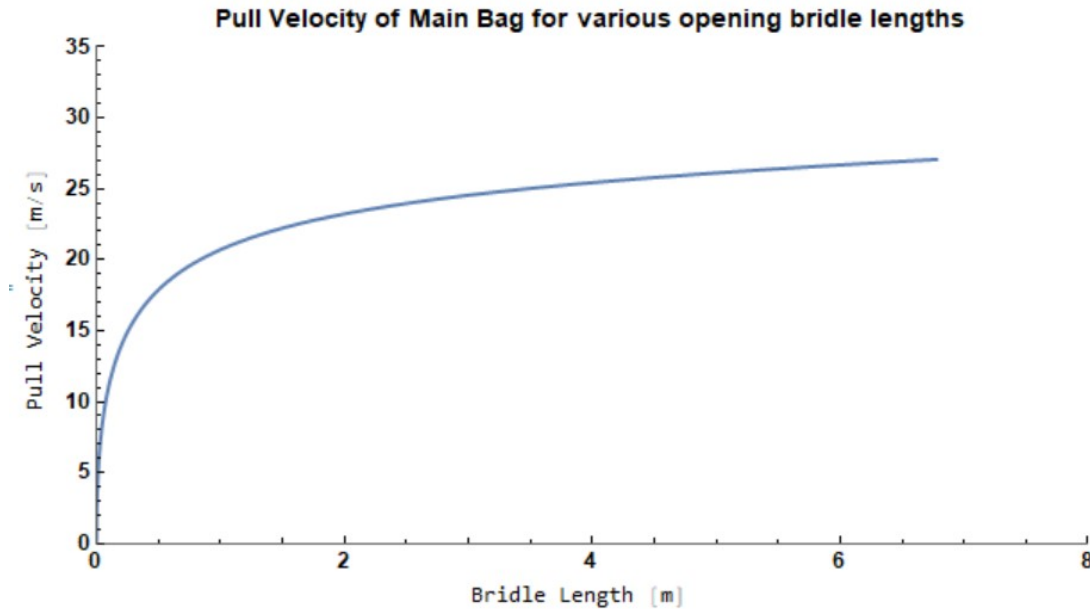
Figure 3.11: Opening Bridle Separation Speed Against Length

The model can and should be extended to include the viscoelastic effects of different cord materials for larger rockets. However, this project deals with relatively low forces and therefore does not require such an in-depth study. What needs to be addressed, however, is the possibility of elevated Snatch Forces and how to deal with them. This is explored in the following Section 3.4.1.

3.4.1   Cords

There are two forces that will directly impact the sizing of the recovery recovery system: drogue chute and main chute opening force, seen in Section 3.3. In order to comply with the low recovery weight constraint and the black powder ejection, a primarily Kevlar based Cord System was deemed necessary due to its higher strength than that of nylon cords for the same strength and its fire resisting properties. However, this comes with the drawback of higher cost and lower elasticity, which can lead to increased Snatch Forces. This will be tackled later in this section. Furthermore, the cords had to be converted into slings to allow for easy rigging of the system. This is, using knots for *HPR* rockets is undesirable as these weaken the cords and severely lower their breaking stress. Lastly, due to advisor recommendation, hollowed tubular kevlar cords were preferred over flat cords due to the reduced risk and severity of fuselage zippering during deployment.

In order to further reduce weight and cost, the lines that are subjected to the drogue opening force of ≈ 1400 N will be constructed out of smaller sized cords. The Main Parachute Riser, on the other hand, will have to sustain ≈ 4200 N, as seen in Section 3.3.

Commercial kevlar slings offered by rocketry companies was an option. However, with the aim of supporting local companies, ClipCarbono$^{©}$'s ≈ 6 mm and ≈ 20 mm diameter tubular kevlar cords were purchased. Unfortunately, they did not specify their breaking strength. However, these sizes where selected by comparing the breaking strength of similar commercial cords. The strength test is evaluated in Section 4.2.1. Figure 3.12 shows the ends of the kevlar slings used in the recovery system

Figure 3.12: Kevlar Slings

Finally, in order to minimize the harder-to-estimate Snatch Forces and the Opening Force, all the parachutes lines are folded and stowed with the help of rubber bands or breaking bands. These both assist in organizing the recovery lines to prevent

tangling during deployment and will slip and or break during deployment and infla-tion. This way, they absorb some component of the energy when re-accelerating the recovery system (Snatch Force) and during parachute inflation. Figure 3.13 shows a Kevlar sling with the installed rubber bands.

Figure 3.13: Rubber bands used to stow the lines and minimize forces

3.4.2 Tender Descender Selection

Commercial Stage Separation systems were desired as this is a critical stage in the recovery procedure. Both small Pyrotechnic Line Cutters and Tender Descenders were considered for this project. However, only the tender descender is compat-ible with this rocket build, as this separation element must sustain the full force of the drogue deployment and the commercial cable cutter cannot deal with such high stresses. The most appropriate model is the Tinder Rocket© L2 Tender De-scender, seen in Figure 3.14. This uses a small black powder charge to forcefully eject the holding pin that secures the two small quicklinks to the orange retainer. Its specifications are listed below.

Figure 3.14: Tinder Rocket© L2 Tender Descender

- Dimensions (no quicklinks): $\approx$ 45x20x20 mm

- Mass (no quicklinks): 52 g

- Maximum Recommended Shock Load: $\approx$ 8900 N

- Maximum Recommended Release Mass: 225 kg

- Maximum Recommended Rocket Mass: 34 kg

3.4.3 Triple Ring Release System

A stage separation device must be light-weight, sustain a high force and require a small input force to activate. These can range from electro-mechanical devices to simple pyrotechnic devices. Reference [2] contains a list, along with diagrams, of several of such devices. The most common system is a pyro activated line cutter. The cord will be attached to a cylinder like element that holds a blade. This blade is forcefully pushed by a small detonation and cuts through the cord. These are also very commonly used in reefing systems. However, when lines become too thick to reliably cut with a small device, a mechanical advantage mechanism is installed. Effectively, the input force needed to 'cut' the line is reduced thanks to this system.

(a) Parachuting 3-ring system

(b) SRAD Triple Ring Release System

Figure 3.15: Comparison between commercial and SRAD 3-ring release system

With the aim of developing a SRAD (self research and developed) stage separation device, a Triple Ring Release System was designed. This technology was developed in the 70s by parachutists to be able to reliably and manually release their emergency parachute. Through the means of mechanical advantage, the relatively small pulling force on the holding cable created a cascading effect that lead to the separation of the system. Figure 3.15a shows a typical parachuting 3-ring mechanism, whereas Figure 3.15b showcases the final device that will be implemented in the *ASTRA* rocket.

A small SRAD pyrotechnic device will activate by means of electronic matches when meeting the Main Parachute Deployment condition. Two matches are used to incorporate redundancy to the event and an extra layer of protection. This event will release the holding cord that loops through the smallest ring. Reference [27] details how the 3-ring mechanism is sized. However, in this project, due to to the

scarcity of options for manufacturing the system, as custom sized welded rings were not on the table, several iterations where constructed with available materials and tested until a suitable configuration was found. This testing is discussed in Section 4.2.4. On a final note, these were made out of 1000 kg strength rated 25mm flat polyester cord instead of the desired kevlar system. They were constructed with the help of the Faraday Rocketry UPV's sponsor *Loadlok©*, and their smallest available cord was the one used in this project. A loose protective sleeve is placed around the 3-ring device to shield the cord from the black powder ejection.

3.4.4   Connectors and other elements

Quicklink and Swivel Selection

As mentioned in section 1.3, connecting elements such as quicklinks and swivel links are designed with a Safety Factor, which will depend on the intended application. In order to reduce weight, it is possible to use connectors that, according to their Safe Load Limit, are not suitable for the project, in order to reduce weight. However, the limiting forces acting on these elements are more closely related to impact stress than of constant pulling. Therefore, it is not as simple just to test their breaking strength in a quasi steady state. This is discussed in Section 4.2.1.

| (a) Selected quicklinks | (b) Selected Drogue Swivel Link |

Figure 3.16: Selected Connectors for the *ASTRA* rocket

While it was possible to purchase 'quick swivel links' that serve both purposes, these were more expensive and due to the odd non-axisymmetric shape, it was believed that they would not support as much load as their simpler counterparts. As such, various sized connectors were strength tested and selected based on their performance. Finally, the Main Parachute already came with its $\approx$ 6650 N rated swivel, so only a swivel was needed for the drogue parachute. Figure 3.16 shows the final connectors selected.

Fireproof sheet and wadding

In order to protect the parachute from the hot gas ejection, the drogue parachute is wrapped around a fireproof blanket, as seen in Figure 3.17a. This element has an eyelet on which the recovery lines can be attached. This way, they protect the chute and fall with the rocket, to be reused. They were purchased from *Madcow Rocketry* and they do not specify the material used.
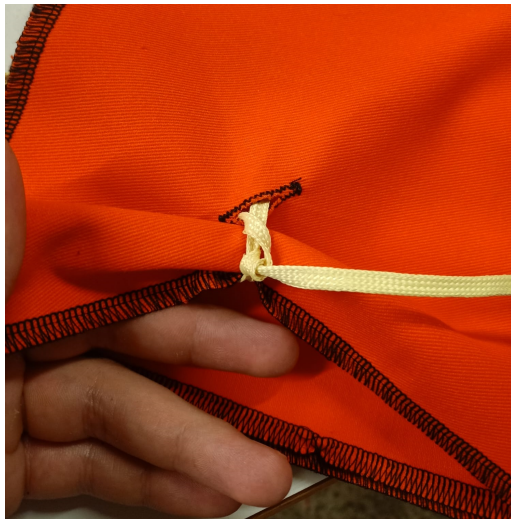
(a) Flame Resistant Parachute Blanket

(b) Recovery Wadding

Figure 3.17: Fireproof protectors

On top of using fire protecting blankets, even though it is not strictly necessary, a second layer of safety is added by incorporating disposable parachute *wadding*, seen in Figure 3.17. This material may come in sheet form or in cotton like fibers that are pressed between the ejection charge and the recovery elements susceptible to flame damage. Both the wadding and the blanket are not shown in the Lines Diagram of Section 3.4 for simplicity reasons.

Main Parachute Bag

The purpose of the Main Parachute Deployment Bag, as explained in Chapter 2, is to both allow for slower proper unfurl of the parachute, which reduces the risk of a higher than expected Snatch Force. Furthermore, it is made our of a similar material to that of the parachute protector blanket and will shield both the parachute and its nylon suspension lines from the black powder charge. A compatible Deployment Bag made for the IFC 72" Iris Ultra Standard Parachute is selected from the same company, as seen in Figure 3.18. Even though it dimensions specify that it must be used for ≈ 100 mm interior diameter, results seen in Section 4.2.5 show that this choice is compatible with the mission requirements.

Figure 3.18: Fruity Chute©'s 4"d x 12"l Deployment Bag Main Parachute.

The shock cord is folded with elastic bands for shock load absorption and then pressed between the deployment bag bands. This way, when the opening bridle pulls on the deployment bag, the main parachute cord will, along with the bands, be pulled away. Once no more cord is left, the deployment bag will open, allowing for the inflation of the Main Parachute. The breaking bands will then absorb this opening force and the subsequent snatch force created by the re-acceleration of the Drogue Parachute lines that attach to the apex of the main chute.

Chapter 4

Testing and Results

4.1 *ASPERA* sub-scale rocket test

In order to acquire sufficient knowledge on the construction of High Power Rockets and to test the recovery procedure with black powder ejection, a smaller sub-scale prototype of the *EuRoC* rocket was designed: *Aspera*, seen in Figure 4.2. It was designed to reach an apogee of 1 km and used a single parachute recovery event.

Figure 4.1: Finalized *Aspera* rocket

- Length: 122.6 cm

- Exterior diameter: $\phi = 94$ mm

- Interior diameter: $\phi = 90$ mm

- Total Mass: 3778 g

- Dry Mass: 3466 g

- Expected Apogee: 930 m

- Recovery Bay Length: 324 mm

- Launch site: "Aeródromo de Ontur"

The diameter was set to be equal to that of its larger successor *ASTRA*. This way, the Manufacturing, Structures and the Recovery Department could better validate their results to be later used on the larger build. As far as recovery is concerned, this model served to test the black powder ejection, inflation models and strength test the 6 mm kevlar cord as well as the swivel and quicklinks, as the same ones are used in for this sub-scale prototype. Due to the difference in mass, a different parachute was implemented for this sub-scale test. The nomenclature of this lines diagram is analogous to that of Figure 3.4, however, the fireproof blanket is shown in this figure.
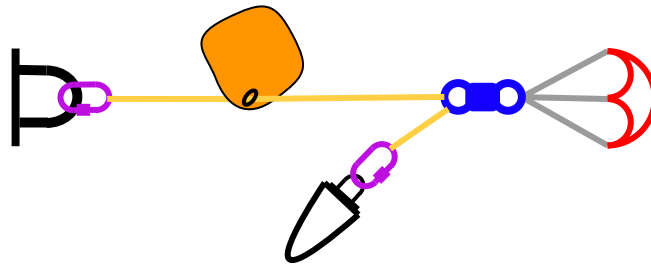
Figure 4.2: *Aspera* lines diagram

Cd0	0.7	Mass [g]	135
D0 [m]	1.37	Packing density [cm^3]	550
S0 [m^2]	1.47	Type	15° Conical
Dp [m]	1.32	Cost + shipment [EUR]	≈ 75

Table 4.1: *Public Missiles*'s PAR-54 inch Parachute

Following the Force Estimation Procedures noted in previous sections, the worst case scenario with a 40 m/s velocity at the moment of inflation lead maximum opening shock force of around 950 N. The low forces involved meant that knots could be used in the rigging process, which simplified the construction process. Experience has shown that the length of the riser cord should be higher than triple the length of the rocket length. As such, a 6 mm Kevlar riser cord of 4 m was used.

4.1.1 Black Powder Ejection

The first step into designing a functional ejection method is the to assure the repeatability of the process. This way, there is no doubt as to how forcefully the recovery system is ejected the day of the launch. It was confirmed during testing that grain size and pressure packing of the black powder charge affected the burn rate and therefore how fast the recovery bay was pressurized.
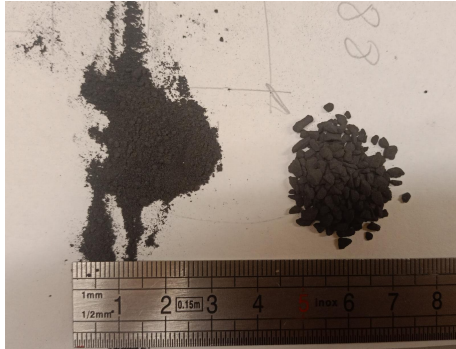
(a) Powdered vs untouched Black Powder
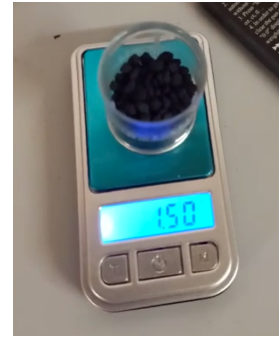
(b) Black Powder Test Charge 1.5 gr

Figure 4.3: Black powder used for ejection testing

Even though successful simple igniters were created using scrap copper cables, testing showed that these failed around 10% of the trials. Hence, the day of the launch, commercial igniters are used to ensure proper performance[1]. Figure 4.4 shows the difference.
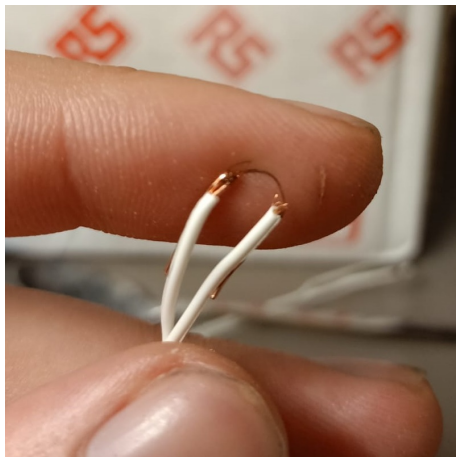
(a) SRAD simple igniter
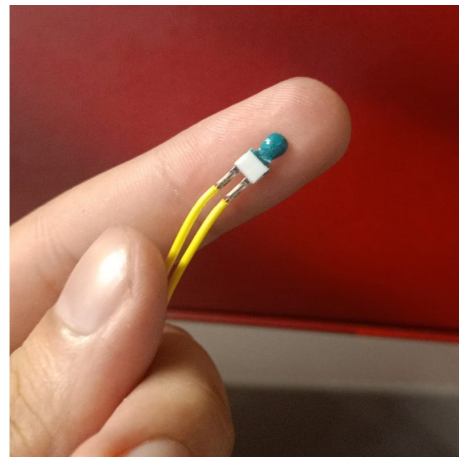
(b) Commercial Igniter

Figure 4.4: SRAD vs Commercial igniter

The most optimal solution found was the following: the measured black powder charge and igniter are encapsulated in a tissue paper and pressed with masking tape to create sufficient pressure.

4.1.1.1 *Aspera* Ground Testing

The test bulkhead, shown in Figure 3.3, is mounted inside a same diameter fiberglass tube and a 1.5 kg mass is placed to visualize how far the recovery would be ejected. As seen in Equation 3.2 in Section 3.2.3, given *Aspera*'s 324 mm of recovery bay length, a black powder charge of 1 g should be enough for 15 psi of internal pressure to be generated to eject the recovery system.

---

[1]Tender Descenders use SRAD Igniters as the acquired commercial igniters do not fit into the charge hole

Figure 4.5: *Aspera* black powder ejection ground test

Testing showed that this charge had to be increased to 2 grams and ground into a fine powder for enough ejection speed to be generated. This could be explained by the igniter surface area and used black powder's exact composition, which was unknown, and could have lead to a different specific heat capacity value. Figure 4.5 also showcases why appropriate thermal protection is needed, as the explosion can easily burn through parachute cloth.

4.1.1.2 *Aspera* Mid-air ejection

This 2 gr black powder charge is then used for a mid-air ejection and inflation test [2]. It is desired for the system to be ejected with enough speed that the riser cord quickly reaches almost its final taught length. However, if too much pressure is used and the riser length is shorter, this can cause a rebound effect that even cause undesirable uneven forces on the system. This is what was tested in these test trials.

Figure 4.6: *Aspera* Drop Test Set Up

A discarded fiberglass fuselage with a 4 kg dummy mass was launched from the top of a 34 m high building with the parachute system installed. Attempts to validate the 0.7 parachute drag coefficient were attempted but parallax error and relatively low drop height generated too much uncertainty to obtain a value within an acceptable margin of error. Solving Equation 3.3, the expected terminal velocity is ≈ 7.4 m/s. A simple *IMU* system to measure the acceleration and velocity during the drop

---

[2]Due to the elevated cost of Kevlar cords, some of the tests were conducted with overestimated polyester rope. Kevlar was used to validate the fact that the knots would hold for *Aspera*'s launch

Figure 4.7: *Aspera* Drop Test Sequence

test was attempted. However, issues with the avionics system from the Avionics Department prevented this tests from taking place. The sequence of the drop tests can be seen in the series of images seen in Figure 4.7.

This specific drop test is shown to illustrate a possible problem that arises with a strictly vertical flight path and the recovery system is ejected ta apogee nose down. As seen in the second still image, ejection occurred very close to apogee. However, as there was no horizontal velocity, there was not sufficient speed to inflate the parachute. The rocket body then must overtake the lighter folded parachute mid air, so it can then pull on the parachute riser and inflate the parachute. This increases the likelihood of zippering the fuselage. This is the reason why it is desired for the recovery system to be ejected nose up or horizontal at most. The low pressure difference at 1 km height withing the recovery bay meant that there was no need for installing shear pins. The tight fit between the nose cone interior lip and the fuselage would be sufficient to prevent premature ejection.

Figure 4.8: *Aspera*'s Parachute Damage by Improper Blanket Shielding from Black Powder Charge

Finally, to further emphasise the importance of adequate thermal shielding to the parachute from the hot gas ejection, in one of the drop tests the parachute was not properly packed with the protective blanket. Thus, the portions of exposed

parachute cloth charred, as seen in Figure 4.8. Thankfully, damage was minimal. Holes were patched and the same parachute was used for *Aspera*'s launch.

4.1.2 *Aspera* Launch and Recovery

The sub-scale prototype was successfully launched the 21st of May 2022. Regarding Recovery, the system was never tested on a high wing environment. The gained horizontal speed from both the slightly angled launch path and windy conditions [3] could have posed a threat to the mission. In order to have sufficient aerodynamic stability, the rocket had to be launched with less than 6.5 m/s (12.5 knots) wind. This wind also increased the drift distance to about 600 meters.

(a) *Aspera* Recovery System Rigging before launch
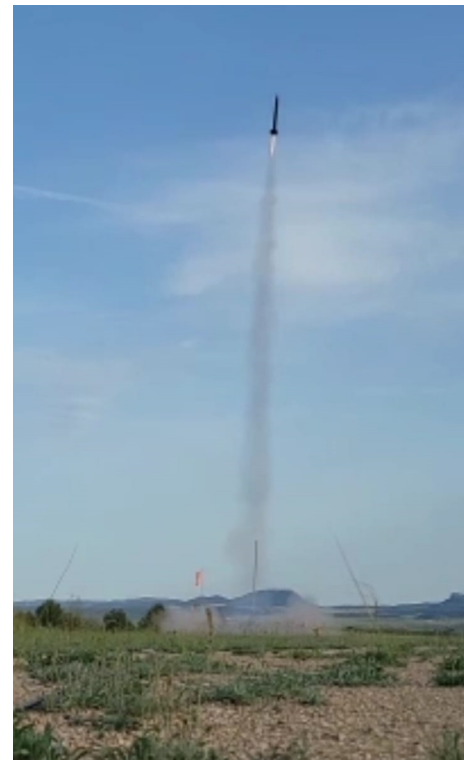
(b) *Aspera* Launch out of Rail

Figure 4.9: *Aspera* Launch

Regrettably, both issues with ground control telemetry the day of the launch and data overflow on the onboard avionics lead to no recovered data. This means that the parachute drag coefficient, acceleration during ejection and recovery were not measured. However, the recovery was successful and from the state of the recovered rocket, seen in Figure 4.10, many conclusions for the parachute performance could be made.

The rocket fell about 450 m from launch site, so drift distance was correctly assessed. The simple bowline knots held the opening forces of the parachutes. The rocket fell pointing nose up in rocky terrain, as expected, so first contact was made by the rocket fins as these presented no damage. The high winds then dragged the rocket

---

[3]Winds at 1 km height could not be estimated, but used ground wind as an indicator of safety.

Figure 4.10: *Aspera* Aftermath Assessment

a few meters while parachute was still falling, which scraped the surface of the fuselage. The only visible concern was the zippering of the fuselage. It can bee seen how the parachute shock cord has ripped 5 cm through the uppermost section of the recovery area. Footage, too low quality to show in this document, demonstrated that ejection took place after apogee, when the rocket was pointing nose down. When the parachute inflated and opposed the downward movement, the straightening of the riser cord teared through the fiberglass tube. Needless to say, as far as Recovery is concerned and given the fact that this was the first ever launch of the team, this mission was a success.

4.2 *Astra* Subsystem Testing

While the *Aspera* mission served to test many aspects of the recovery system, some others require individual testing for its use in the *Astra* project. This section deals with the results of all the elements that form the Dual Parachute Recovery Mechanism. Unfortunately, both the parachute opening force and the system as a whole (drop test) could not be tested in time for the resolution of this document due to issues like time delays with the delivery of the parachutes, budget constraints and delays on the rocket construction. Nevertheless, Section 4.4.1 explains all the further testing that will be performed before the rocket launch. Additionally, Section 4.4.2 expands on all the future projects that could be carried out using the information shown in this document as a basis.

4.2.1 Tensile Test and Breaking Strength

In order to test the breaking strength of the connectors used in the construction of this recovery system, both an *Instron*© 1175 Universal Testing Machine and an industrial platform scale, seen in Figures 4.11a and 4.11b respectively, were used. The universal testing machine could better determine the breaking strength of the

cord. However, this was done at a quasi-steady state, whereas the industrial scale, coupled with a forklift, could offer higher speed tests. The forklift raised a 1025 kg mass off the scale using the tested connector, where the difference in mass measured would indicate how much stress the mechanism is sustaining. Needless to say, parachute snatch and opening forces are very sharp in nature and this could have been better tested with a modified *Charpy* Impact Testing Machine. This was not an option and the best was done with the available resources.

(a) *Parafly*'s *Instron*© machine used to test the breaking strength of the Kevlar slings.

(b) *Loadlok*©'s Indutrsial Scale used to test the Connectors.

Figure 4.11: *Instron*© machine and Industrial Scale used for Strength Testing

4.2.1.1 Kevlar Cord Loading

Before assessing the breaking strength of the cords, the elastic behaviour of the slings were evaluated. Due to budget limitations, this test could not be repeated to get an order of magnitude of the cord's spring constant due to the kevlar cost. 6 mm Kevlar slings were hanged from the concrete ceiling, an incremental load was applied and its elongation measured, as seen in Figure 4.12.

(a) 2 kg load.

(b) 14 kg load.

Figure 4.12: 6mm Kevlar elongation measurement attempt

Testings showed that the cords had an elongation far greater than expected. However, this behaviour was plastic in nature in the sense that the cord did not regain its original length. After a certain level of deformation, the Kevlar began to behave with a much higher spring constant. Resulting graph is not shown due to the low fidelity of the testing. However, it demonstrates that non-used kevlar cords will lead to less damaging snatch forces due to this initial deformation.

In both tests, it was the cord itself that broke and not the seam, which confirms that the sling was properly sewed.

6 mm Kevlar breaking strength

This 6 mm Kevlar cord was also tested with a simple bowline knot instead of a sling seam to visualize the strength reduction. In all three cases, the cord broke by the knot.

- Industrial Scale with Forklift:

- 120 kg

- 105 kg

- 115 kg

Combined average breaking strength: 113.3 kg ($\approx$ 1100 N).

- *Instron*$^©$:   - Industrial Scale with Forklift:

- 330 kg   - 325 kg

- 350 kg   - 330 kg

- 345 kg   - 315 kg

Combined average breaking strength: 332.5 kg ($\approx$ 3250 N).

This shows that, at least the typical bowline knot, causes a strength reduction of almost two thirds of that of the pure kevlar cord.

20 mm Kevlar breaking strength

- *Instron*$^©$:   - Industrial Scale with Forklift:

- 970 kg   - 980 kg

- 980 kg   - 965 kg

- 960 kg   - 995 kg

Combined average breaking strength: 975 kg ($\approx$ 9550 N).

Both sling breaking strengths demonstrate that the cords have been properly selected for their use in the *Astra* recovery system based on their maximum expected tensile stresses of $\approx$ 1400 N and $\approx$ 4250 N for the drogue and main parachute opening force, respectively.

4.2.1.2 Connector Loading

Due to time constraint, it was not possible to use the more exact and professional option of the *Instron*© machine. In this case, only the forklift method was an option. Figure 4.13 shows how the elements were connected for the test.

Figure 4.13: *Loadlok*© Swivel Strength Testing Rigging.

The three stainless steel ϕ 5 mm swivels and the three ϕ 5 mm quicklinks could support the full weight of the 1025 kg mass ($\approx$ 10000 N). Even under very visible plastic deformation (Figure 4.14), the swivel could still rotate and the quicklinks could still open with the use of pliers. Given the fact that these elements had to sustain the same drogue opening force of $\approx$ 1400 N, it is safe to say that these elements are a valid solution for the requirements of the mission. Even though the smaller quicklink could also support the load of the main parachute, for safety reasons it was decided to overestimate and use the larger ϕ 8 mm model.

(a) Swivel

(b) Quicklink

Figure 4.14: Connector Deformation after applied 1025 kg load.

4.2.2 Shear Pin Testing

Instead of buying commercially available shear pins, it was decided to create our own version. These elements, as explained at the end of Section 1.4, must sustain the over-pressure inside the recovery bay to prevent premature nosecone ejection. The calculation of maximum estimated pressure difference was given in section 3.2.1, where the bottom of the nose cone would have a maximum of 200 N at 3 km height. As a result, a mechanism that could hold 200 N of force and cleanly break with a shearing force past this load was determined.

(a) Close up of Fuselage hole and broken pin

(b) Test Set up Up just before breaking under $\approx$ 20 kg

Figure 4.15: Shear Pin Test Set Up

After several iterations, simple 1 cm length 3D printed PLA plastic cylinders of $\phi = 2.5$ mm were deemed the best solution. Three holes where drilled on a model nosecone and a discarded kevlar fuselage. The system was hanged by a pull scale and weight was added to the end of the system where the tree pins had to support the full weight of the mechanism, as seen in Figure 4.15b. Even though this is not an exact simulation of the conditions, it serves its purpose in determining a system that will shear break past 200 N of applied loading. The pins did not tear through the nosecone bulkhead and kevlar fuselage, as seen in in Figure 4.15a.

4.2.3 Tender Descender Testing

Even though this was a commercial system, the component was still tested to ensure proper performance the launch. The system was hanged from the ceiling and a 13 kg load was connected on the other quicklink. The head of the commercial electronic match was too big to fit the already made hole. The hole was widened to allow the igniter to properly lit the powdered black powder charge of 1 gram. This larger hole and big igniter head lead to too much pressure escaping through this cavity as seen in Figure 4.16a. The smaller SRAD igniter with duct tape lead, seen in Figure 4.16b to successful separation in all cases.

(a) Failed Test
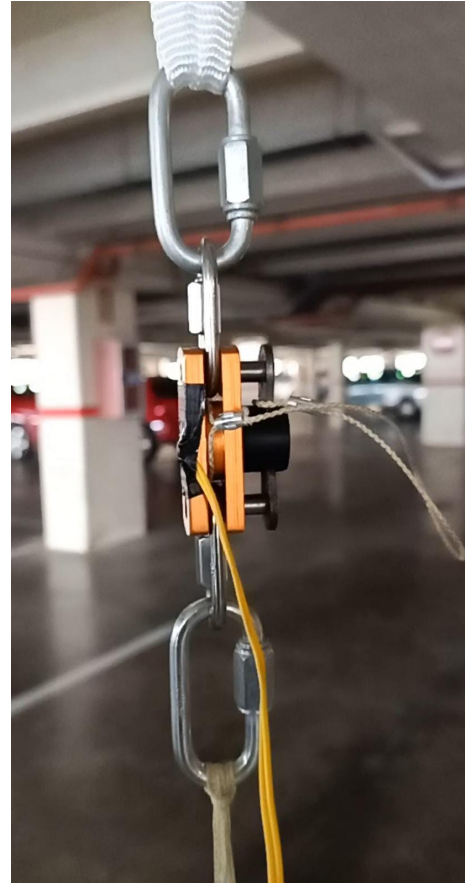
(b) SRAD Igniter for better performance

Figure 4.16: Tender Descender Testing

Finally, given the small size of the tender descender quicklinks, the shock resistance was assessed by dropping the same 13 kg mass from various heights to ensure that it could sustain the calculated 1400 N upper limit for the Drogue Chute Opening Force. As seen in Section 3.4.2, the L2 Tender Descender can sustain up to 9000 N of shock loading. The shock loading can be estimated using Equation 4.1, where gravitational potential energy is divided by the moved distance.

$$F = \frac{mgh}{d} \tag{4.1}$$

To ensure the 1400 N limit was surpassed given the difficulty of measuring the energy dissipated in every element of the system, the 13 kg was dropped from 2 m height. Slow motion video footage and extension of the kevlar cords led to an estimated elongation of around 5 cm. This corresponds to a shock load of around 5100 N. As such, this element complies with the demands of the mission.

4.2.4 Triple Ring Testing

As seen in Section 3.4.3, this device serves the same purpose as the L2 Tender Descender: cutting the drogue line to allow for Main Parachute Deployment. Material

availability did not allow the selection of custom sized rings. Ideally, continuous non welded rings would be preferred as these can sustain higher stresses. However, these were both very expensive and difficult to find with the desired diameter. As such, stainless steel rings of sizes ranging from ϕ 90 mm to 20 mm where bought. With the help of the team sponsor *Loadlok*©'s resources, several triple ring iterations were manufactured. These where done their polyester 25 mm wide flat cord that is rated at 1000 kg with a safety factor of 7. Even though this cord is overdimensioned, due to the amount of testing required and the price of kevlar cord, this what the best solution. As polyester can burn or lose mechanical properties with the heat of the ejection, the system is shielded with a loose protective blanket similar to the used for the parachute deployment. Figure 4.17 shows the evolution of the first version (blue) to the final iteration of the triple ring system (orange).

Figure 4.17: Comparison of First Triple Ring Prototype (Blue) and Final Version (Orange).

All the prototypes where strength tested following the same procedure seen in Section 4.2.1. The a mass of over 750 kg was lifted with a forklift with the triple ring as the connection point. As such, the mechanism will confidently comply with the calculated drogue loading.

(a) Testing Set Up

(b) Pull Scale measuring holding force

Figure 4.18: Triple Ring leveraging factor test set up

The system also had to be able to release with the tension in the string during the main parachute deployment phase. The tension in the string will be equal to the mass of the falling rocket. The force reduction of the leveraging mechanism was tested by means of attaching a 13 kg mass to one end of the polyester sling where the other end sling was attached to a stiff rod that would hold the weight. A pull scale was used to hold the smallest ring. On average, the force acting on the scale before the cascading effect took place was 4 N. The force to confidently pin the smallest ring to the initial position was around 9 N. Therefore, this SRAD triple ring, at only 60 gr mass with the igniter attached, has a maximum leveraging factor of ≈ 32. This means that the igniter pin must only exert a holding force of around 4 N. Further testing, showed that this igniter system successfully allows for separation of the holding pin, leading to the uncoupling of the mechanism.

4.2.5 *Astra* Ground Testing

Ground testing is performed to ensure that all the lines and parachutes fit the required tube length and that the ejection force is enough to break the shear pins and push the recovery system sufficiently. Figure 4.19 shows the first ejection trial. This image is shown to illustrate the importance of ground testing the recovery system before drop testing can take place. In this case, too the snug fit of the main parachute bag acted as a sort of piston head, whereas in *Aspera*, some pushing force was 'lost' as gases almost filled the volume before actual nosecone separation took place. As a result, instead of the 2.5 gr of black powder, the charge was reduced to 2 gr. In all cases, the shear pins broke and the shielding agents protected the flamable elements.

Figure 4.19: Ground Testing with only Main Parachute Bag

4.3 Final Configuration

This section will list all the used equipment for the creation of this dual deployment recovery system seen in Figure 3.4. If one wishes to recreate this model and these particular elements cannot be found, the specifications they must comply with are also noted. It is up to the reader to understand the the specific technical requirements of their design and modify this model as they see fit.

ϕ 8 mm Quicklink

- **Quantity:** 2
- **Weight/unit:** 71 g

- **Material:** Stainless Steel
- **Min. Strength:** >10000 N

ϕ 5 mm Quicklink

- **Quantity:** 5
- **Weight/unit:** 20 g

- **Material:** Stainless Steel
- **Min. Strength:** >4000 N

ϕ 5 mm Swivel link

- **Quantity:** 1
- **Weight/unit:** 35 g

- **Material:** Stainless Steel
- **Min. Strength:** >4000 N

The used IFC 72" Iris Ultra Standard Parachute already has a installed ball swivel link. This swivels is for the drogue parachute.

L2 Tender Descender

- **Quantity:** 1

- **Weight/unit:** 58 g

- **Material:** Stainless Steel + Aluminum
- **Min. Strength:** >4000 N

Triple Ring Mechanism

- **Quantity:** 1

- **Weight/unit:** 60 g

- **Material:** Stainless Steel + 25 mm flat polyester
- **Min. Strength:** >4000 N

Alternatively, a second L2 Tender Descender can be used, also connected in series.

4"d x 12" l *Fruity Chutes* Main Parachute Bag

- **Quantity:** 1
- **Weight/unit:** 80 g

- **Material:** Fire Resisting Cloth
- **Min. Strength:** -

Shear Pins

- **Quantity:** 3
- **Weight/unit:** 1 g
- **Material:** PLA Plastic
- **Combined Shear Force:** 200 N

Black Powder

- **Total Quantity:** 6 g

Electronic Match

- **Quantity:** 5
- **Weight/unit:** 3 g
- **Head Resistance:** 1.5-1.7 Ω
- **Firing Current:** 1 A

6 mm hollow tubular Kevlar slings

- **Quantity slings:** 1 m and 5 m
- **Quantity Cord:** 2 m
- **Weight:** 3 g/m
- **Material:** Kevlar 49
- **Min. Strength:** >4000 N

20 mm hollow tubular Kevlar slings

- **Quantity slings:** 5 m
- **Weight:** 5 g/m
- **Material:** Kevlar 49
- **Min. Strength:** >8000 N

Fruity Chutes IFC 72" Iris Ultra Standard Parachute

- **Quantity:** 1
- **Weight/unit:** 376 g
- **Material:** 1.1oz mil-spec calendared ripstop nylon
- **Min. Strength:** >6600 N

A parachute that can also fit the deployment bag an the fuselage with similar opening forces and terminal velocity may also be employed.

Decelerator/Drogue ϕ 0.72 m Parachute

- **Quantity:** 1
- **Weight/unit:** 108 g
- **Material:** mil-spec nylon
- **Min. Strength:** >4000 N

A parachute that can also fit in the fuselage with similar opening forces and terminal velocity may also be employed.

Parachute Cloth Protector Blanket

- **Quantity:** 15 cm * 15 cm
- **Material:** Flame Resistant Cloth
- **Weight/unit:** 40 g
- **Min. Strength:** -

Parachute wadding

- **Quantity:** ≈ 20 g

Total Weight: 1208 g
Total Length: 450 mm

4.4 Future Testings and Projects

4.4.1 Future Testings

Just as the recovery system for the sub-scale prototype *Aspera* was performed by a drop test, the same should be done for its larger predecessor. This drop test requires at least 100 meters of height to fully test the opening of both parachutes. By means of an airdrop attempt with a Helicopter or Drone, this test would be achievable. In the case of this project, a drone drop test will be performed at 120 m elevation in September, which is the maximum allowed height for cargo drop testing in Spain as seen in the EASA document: Easy Access Rules for Unmanned Aircraft Systems (Regulation (EU) 2019/947 and Regulation (EU) 2019/945), page 135 [28].

4.4.2 Possible Future Projects

This end of degree project deals with many aspects of the recovery phase of sounding rockets and, a such, has great potential for future more in-depth specific research and practical essays. In this section, a list of possible projects that can arise from the theoretical and practical ground of this work is shown below.

- *CFD* analysis of transient behaviour during parachute inflation.

- Wind Tunnel testing for light airborne parachute systems

- Visco-elastic properties of different parachute cloth and cord materials.

- Effects of parachute size on $C_k - R_m$ dependency.

- Extension of Ludtke Inflation Model for vented parachutes.

- Development of a parachute stage separation device by means of mechanical advantage.

- Montecarlo simulation for parachute forces with interpolated semi-empirical data.

Conclusion

This project has dealt with the design and testing of a parachute recovery system for an experimental sounding rocket, implementing parachute inflation theory and aerodynamic modelling. Just the sheer number of studies and propositions for parachute modelling prove the difficulty involved with these systems. There are a great deal of variables involved in the inflation process. Coupled with the unavoidable degree of randomness that arises with the deployment and the central nature of the recovery phase of a rocket launch makes this field engineering as hard as it gets. My contribution has been the creation of an up to date state of the art of both the theoretical and methodological backgrounds that make these mechanisms possible. At the same time, I have applied these concepts to arrive at a simple and cost effective yet well-rounded parachute recovery system that complies with all the requirements imposed by both internal and competition constraints. The success of the sub-scale prototype *Aspera* launch demonstrate that the theory work, testing and the manufacturing process have been valid, and that these results can be extended to the final version of the recovery system. I have no doubt that the *Astra* rocket well perform a successful recovery at *EuRoC* 2022.

During my work, I found that the most limiting factors were the resources available, time management, unavoidable delays and unexpected challenges in the likes of cost increases and surprising ambiguity of some legislations. These are all well-known to veteran engineers. However, this has been my first ever contact with said problems and it has been a great source of learning, given the fact that these are not usually faced in conventional university work. Studying this degree has taught me information and given me abilities that were essential to the development of this project, namely knowledge about Aerodynamics, Material Science, Mechanics and Fluid Dynamics. Nevertheless, the creation of this Recovery System had a very steep initial learning curve that posed a very satisfying challenge. I expect my work to be useful for the development of future projects that deal with similar challenges as well as serve as a basis for more in-depth research.

Appendix A

Project Budget

This appendix shows the total cost of both the research phase and the construction of the parachute recovery system seen in this work. It must be stated that both many materials and tests were done with the help of sponsoring companies, namely the strength testing of materials and drogue parachute, so was no the real cost.

A.1   Personnel Costs

This section quantifies the total man hours employed for the development of this project. For simulation purposes, the staff is the author at a rate of 24 Euros per hour.

- Staff: 24 EUR/hr

- Hours worked: 750 hours

- Cost: 18.000 EUR

Total Staff Cost: 18.000 EUR

A.2   Depreciation Cost

Laptop

- Cost: 900 EUR

- Hours worked: 500 hours

- Estimated life expectancy: 13.000 hours

- Depreciation: 3.8%

- Cost: 34.61 EUR

PC Screen

- Cost: 250 EUR

- Hours worked: 350 hours

- Estimated life expectancy: 13.000 hours

- Depreciation: 2.6%

- Cost: 6.73 EUR

Total Depreciation Cost: 41.34 EUR

A.3 Material Cost

Only the cost of the material directly applicable to the design, validation and construction of the system is noted below. As such, elements like the discarded fiberglass tubes made by the team's Manufacturing Department that were used for several tests are omitted. Furthermore, scrap materials used for the testing phase like discarded copper cables to make the SRAD igniters are also omitted. Finally, the cost of shipment added to the final cost of each element.

- ϕ 8 mm Quicklink

  - Quantity: 6

  - Cost per unit: 4 EUR

  - Cost: 24 EUR

- ϕ 5 mm Quicklink

  - Quantity: 10

  - Cost per unit: 2.5 EUR

  - Cost: 25 EUR

- ϕ 5 mm Swivel

  - Quantity: 6

  - Cost per unit: 3 EUR

  - Cost: 18 EUR

- *Aspera* ϕ 5 mm Eye connector

  - Quantity: 3

  - Cost per unit: 1.5 EUR

  - Cost: 4.5 EUR

- *Aspera* M6 U-Bolt

  - Quantity: 2

  - Cost per unit: 4 EUR

  - Cost: 8 EUR

- 25 m Duct Tape
  - Quantity: 1
  - Cost per unit: 7.5 EUR
  - Cost: 7.5 EUR
- 45 m Masking Tape
  - Quantity: 1
  - Cost per unit: 4 EUR
  - Cost: 4 EUR
- 10 m Electrical Tape
  - Quantity: 1
  - Cost per unit: 2 EUR
  - Cost: 2 EUR
- Electrical igniters EMP-NO-A2
  - Quantity: 30
  - Cost per unit: 0.3 EUR
  - Cost: 9 EUR
- Black Powder
  - Quantity: 100 gr
  - Cost per kg: 100 EUR
  - Cost: 10 EUR
- 6 mm hollow tubular kevlar cord
  - Quantity: 100 m
  - Cost per meter: 1.05 EUR
  - Cost: 140 EUR
- 20 mm hollow tubular kevlar cord
  - Quantity: 25 m
  - Cost per meter: 1.80 EUR
  - Cost: 75 EUR
- *Public Missiles ltd.* PAR-54 parachute
  - Quantity: 1 m
  - Cost per unit: 55 EUR
  - Cost: 75 EUR

- *Fruity Chutes* IFC 72" Iris Ultra Standard Parachute with 4"dx12"l Deployment Bag

    - Quantity: 2 of each

    - Cost per unit: 280 + 55 EUR

    - Cost: 950 EUR

- Drogue Parachute[1]

    - Quantity: 1

    - Cost per unit: 30

    - Cost: 60 EUR

- Triple Ring Release Steel Rings

    - Quantity: 3 of each size

    - Purchased Sizes: ϕ 20mm:5mm:90mm

    - Cost: 50 EUR

- 25 mm wide Flat polyester cord

    - Quantity: 5 m

    - Cost: 4 EUR

- ϕ 90 mm interior PVC pipe

    - Quantity: 2 m

    - Cost: 5 EUR

- ϕ 20 mm interior PVC pipe (Black Powder Charge Well)

    - Quantity: 1 m

    - Cost: 2 EUR

Total Material Cost: 1473 EUR

A.4 Outsourcing Costs

- *Instron*© Machine Strength Test: 60 EUR

- Forklift and industrial scale: 90 EUR

Total Outsourcing Costs: 150 EUR

---

[1]This is a Fruity Chutes Alternative as the personnel parachute used is not up for sale for normal people.

A.5 Indirect Costs

These are normally accounted for by adding a 25% increase to the total costs thus far in the budget. So far, the costs are: 19623 EUR.

Indirect Costs: 4905.75 EUR

A.6 Total Costs

- **No VAT:** 24528.75 EUR
- **21% VAT:** 29679.79 EUR

Appendix B

Technical Conditions

This appendix expands on the information provided in Section 4.3 by including the conditions on which the recovery system must be tested and employed.

B.1   Quality Control

As this is an experimental rocket, there is no specific quality control that must be done to ensure proper functioning. As long as the elements comply with the mechanical and technical requirements shown in Section 4.3 and are properly tested before the rocket launch following the experiments described in Chapter 4, the system is able to achieve a successful recovery.

B.2   Testing Conditions

It is up to the reader to understand the safety and legal implications of an experimental rocket launch. Thus, this work will only explain the safety regulation and legal framework for testing the parachute recovery system.

This project uses black powder and electrical igniters for stage separation and ejection. This is a potential hazard that is subjected to many regulations under Spanish Law, namely the BOE 12054: "Real Decreto 989/2015, de 30 de octubre, por el que se aprueba el Reglamento de artículos pirotécnicos y cartuchería" and "Recomendaciones de las Naciones Unidas relativas al transporte de mercancías peligrosas, Reglamentación Modelo; Volumen I".

- The person manipulating the black powder charge and igniter must hold at least the "carnet de aprendiz" compatible with "Real Decreto 989/2015". Alternatively, a "AE" certificate for rechargeable firearms may also be used.

- When arming the black powder charge, face masks, safety googles and protective gloves must be worn at all times.

- The arming of the Black Powder Charge must be done away from any heat or electrical source.

- The black powder must be stored in a dry environment in a tight sealed container away from any potential sources of heat and electricity.

- Ground Testing must be done at a minimum safe distance of 8 meters.

Moreover, the breaking strength test in Section 4.2.1 made use of a forklift. This is a dangerous piece of machinery that must be used by a Forklift Certified worker. This person must hold, as described in Article 2.1 of Annex II in the "Real Decreto 1215/1997" document, a type B certificate.

- Due to shrapnel hazard, everyone in the vicinity must use protective googles to prevent eye damage.

- A safe distance of 8 meters from the forklift must be maintained.

Appendix C

Stabilizing Moment Versus Angle of Attack

Figure C.1 shows the evolution of $\frac{\partial C_m}{\partial \alpha}$ with varying angle of attack for various type of parachutes.
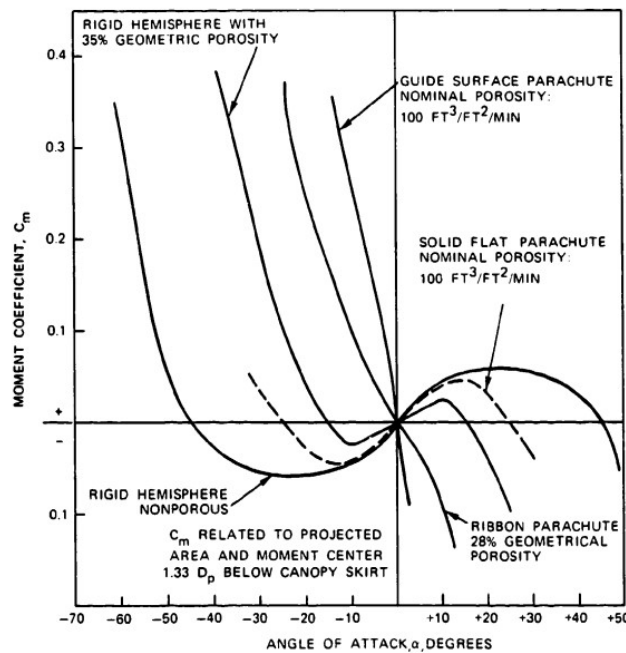

Figure C.1: Moment Coefficient Versus Angle of Attack for various types of parachutes [3]

As mentioned, it is desired for this value to be negative so the oscillation are dampened. Different types of parachutes offer distinct levels of stability. These instabilities may cause stresses on the parachute cloth that need to be taken into consideration. They will also affect the falling trajectory of the rocket, making the drop site more difficult to estimate.
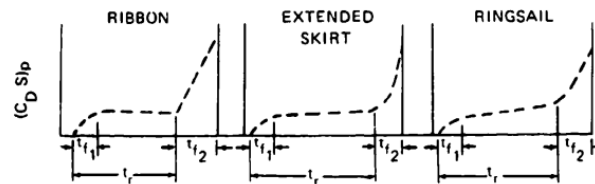
Appendix D

Pflanz Inflation Method - n selection

Figure D.1 shows the typical drag area evolution with inflation time, for both reefed and unreefed parachutes. In Pflanz method, the X_1 parameter has three interpolated curves depending on the drag area profile of the parachute at hand. In the case of unreefed parachutes, the first two types would correspond to the $n = 1$. The third type corresponds to $n = 2$ and the last one is $n = \frac{1}{2}$.
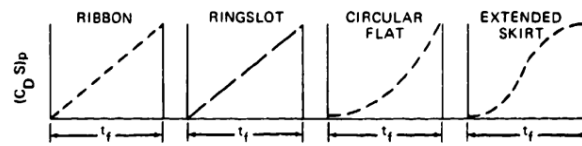
(a) Unreefed Parachutes

(b) Reefed Parachutes

Figure D.1: Drag Area Evolution Profile for various types of parachute configuration

Appendix E

Ludtke High Ballistic Parameter Force Calculation

In the case of higher Ballistic Parameters, where the maximum force occurs in the elastic phase of inflation, when the inertia of the drag air over-expands the parachute cloth briefly. Thus, the visco-elastic effects of the parachute cloth must be taken into account to estimate the openning force. To illustrate this procedure, the method explained in Reference [15] is followed with the help of *Wolfram Mathematica*.
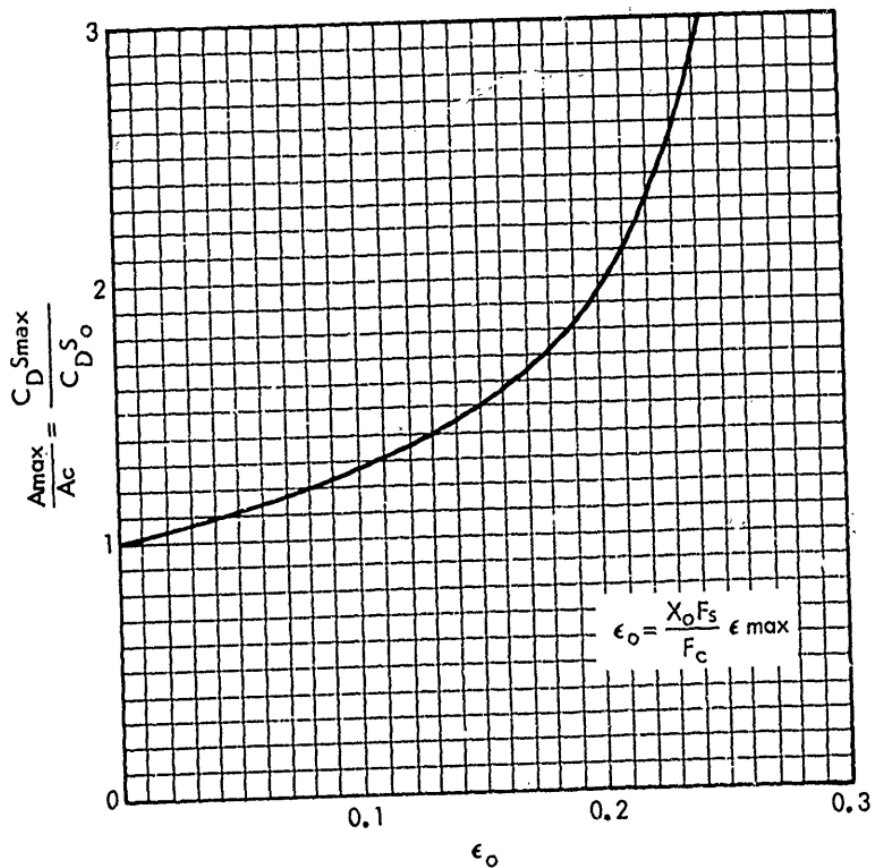

Figure E.1: Maximum Drag Area Ratio Versus Initial Elongation [15]

This method takes into account many parameters that are difficult to know for commercial parachute, such as the strength construction factor, which takes into account the safety factor given to the parachute cloth to sustain the inflation forces, and the maximum elongation of the canopy material. In this case, the same 1.75 safety factor and 0.25 maximum elongation value are used. Figure E.1 is needed to follow the calculation.

In the end, an inflation time of 0.0143 s is found, which leads to an opening coefficient $X_1 = 1.454$ at a time ratio $\frac{tf}{t0} = 1.102$. This amounts to a Maximum Force of 1205 N. Even though many assumptions were done, the same order of magnitude as the other methods for the opening force is obtained.

Appendix F

Canopy Fill Constant - Tabulated Values

In order to calculate the inflation time of a parachute for Equation 2.1, a suitable canopy fill constant is needed. Each parachute inflates at a different rate, and this behaviour is encapsulated with this dimensionless parameter. The typical values are found in Figure F.1 from Reference [3].

Parachute type	Canopy fill constant, n		
	Reefed opening	Disreef opening	Unreefed opening
Solid flat circular	ID[a]	ID	8
Extended-skirt, 10%	16-18	4-5	10
Extended-skirt, full	16-18	7	12
Cross	ID	ID	11.7
Ribbon	10	6	14
Ringslot	ID	ID	14
Ringsail	7-8	2	7
Ribless guide surface	. . .	. . .	4-6

[a] ID = Insufficient data available for meaningful evaluation.

Figure F.1: Canopy Fill Constant tabulated values [3]

Toroidal parachutes, like the main parachute used in this project, have no tabulated canopy fill constant. However, the airflow recirculation caused by the canopy shape of these parachutes lead to the assumption that these inflate quicker than unreefed solid flat circular parachutes. Therefore, a conservative value of $n = 4$ was used in the calculation. Ideally, wind tunnel testing may show a similar trend for these types of parachutes. It is left as a proposition in Section 4.4.2.

Appendix G

Solid Textile Parachute Characteristics

TABLE 5-1. Solid Textile Parachutes.

TYPE	CONSTRUCTED SHAPE		$\frac{D_c}{D_o}$	INFLATED SHAPE $\frac{D_p}{D_o}$	DRAG COEF C_{D_o} RANGE	OPENING FORCE COEF C_x (INF MASS)	AVERAGE ANGLE OF OSCILLATION, DEGREES	GENERAL APPLICATION
	PLAN	PROFILE						
FLAT CIRCULAR			1.00	0.67 TO 0.70	0.75 TO 0.80	~1.7	±10 TO ±40	DESCENT, OBSOLETE
CONICAL			0.93 TO 0.95	0.70	0.75 TO 0.90	~1.8	±10 TO ±30	DESCENT, M < 0.5
BICONICAL			0.90 TO 0.95	0.70	0.75 TO 0.92	~1.8	±10 TO ±30	DESCENT, M < 0.5
TRICONICAL POLYCONICAL			0.90 TO 0.95	0.70	0.80 TO 0.96	~1.8	±10 TO ±20	DESCENT, M < 0.5
EXTENDED SKIRT 10% FLAT			0.86	0.66 TO 0.70	0.78 TO 0.87	~1.4	±10 TO ±15	DESCENT, M < 0.5
EXTENDED SKIRT 14.3% FULL			0.81 TO 0.85	0.66 TO 0.70	0.75 TO 0.90	~1.4	±10 TO ±15	DESCENT, M < 0.5
HEMISPHERICAL			0.71	0.66	0.62 TO 0.77	~1.6	±10 TO ±15	DESCENT, M < 0.5, OBSOLETE
GUIDE SURFACE (RIBBED)			0.63	0.62	0.28 TO 0.42	~1.2	0 TO ±2	STABILIZATION, DROGUE, 0.1 < M < 1.5
GUIDE SURFACE (RIBLESS)			0.66	0.63	0.30 TO 0.34	~1.4	0 TO ±3	PILOT, DROGUE, 0.1 < M < 1.5
ANNULAR			1.04	0.94	0.85 TO 0.95	~1.4	< ±6	DESCENT, M < 0.5
CROSS			1.15 TO 1.19	0.66 TO 0.72	0.60 TO 0.85	1.1 TO 1.2	0 TO ±3	DESCENT, DECELERATION

Figure G.1: Solid Textile Parachute Performance and Characteristics [3]

Appendix H

ASTRA Parachute Force Calculation

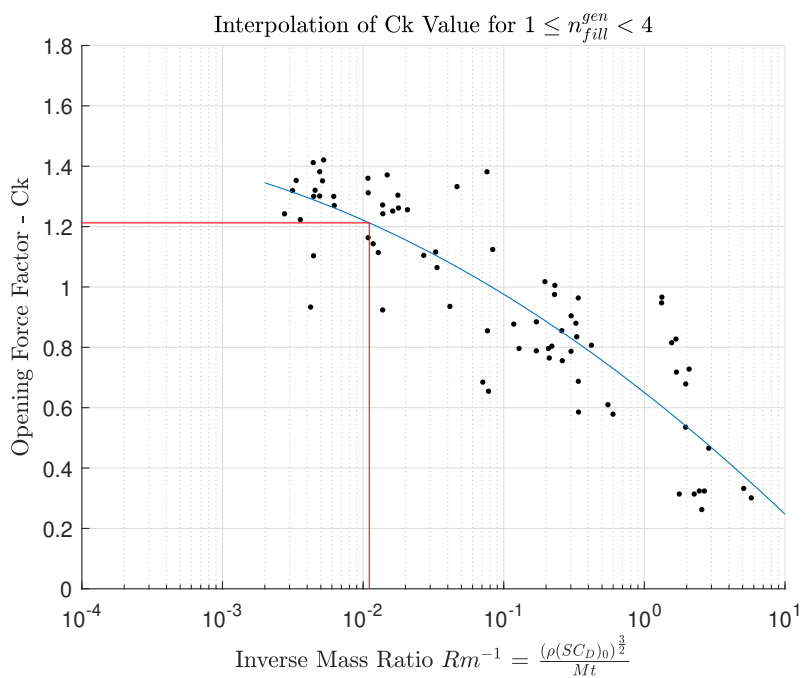## H.1   Drogue Parachute Calculation

Figure H.1: Drogue Parachute Interpolation of C_k following Moment-Impulse Theorem [19]

- generalized non-dimensional filling time: 1.079

- Drag Area Integral: 0.2

- MGI Integral: 0.0074386

- C_k analytic estimation: 1.246
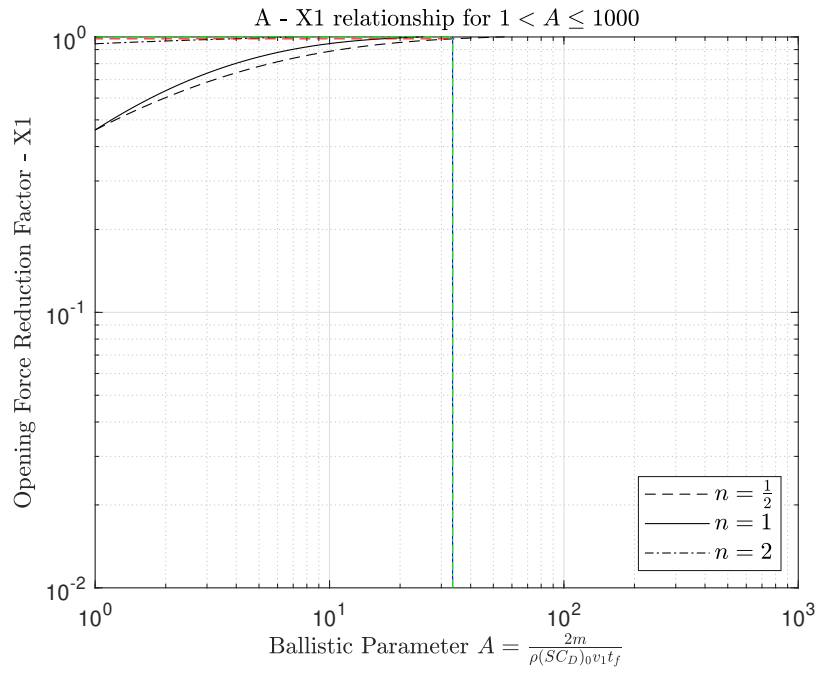
- F_{max} analytic estimation: 1033.14 N

Figure H.2: Drogue Parachute Estimation of X_1 following Pflanz Method [3]
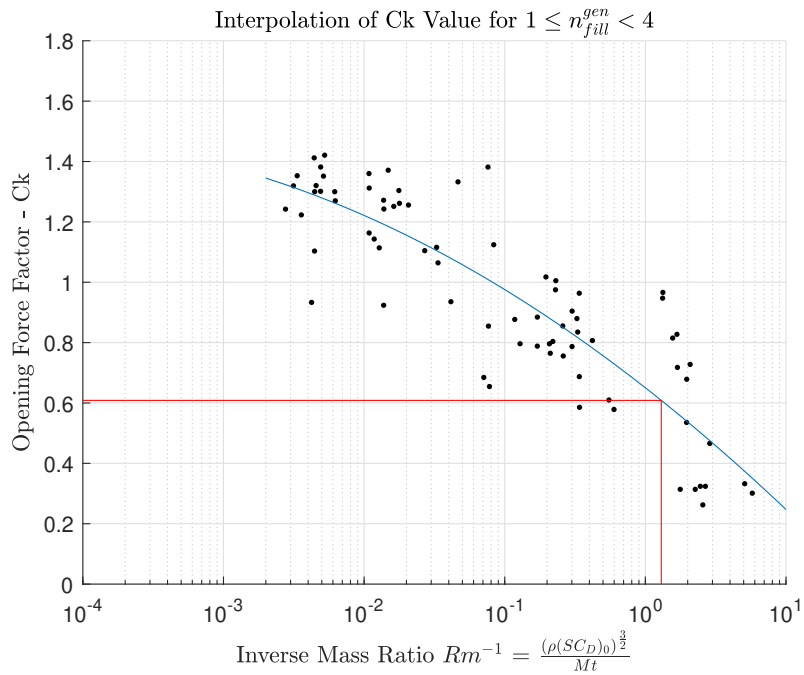
H.2 Main Parachute Calculation

Figure H.3: IFC 72" Iris Ultra Standard Parachute Interpolation of C_k following Moment-Impulse Theorem [19]

- generalized non-dimensional filling time: 1.217

- Drag Area Integral: 0.4

- MGI Integral: 0.3438

- C_k analytic estimation: 0.435
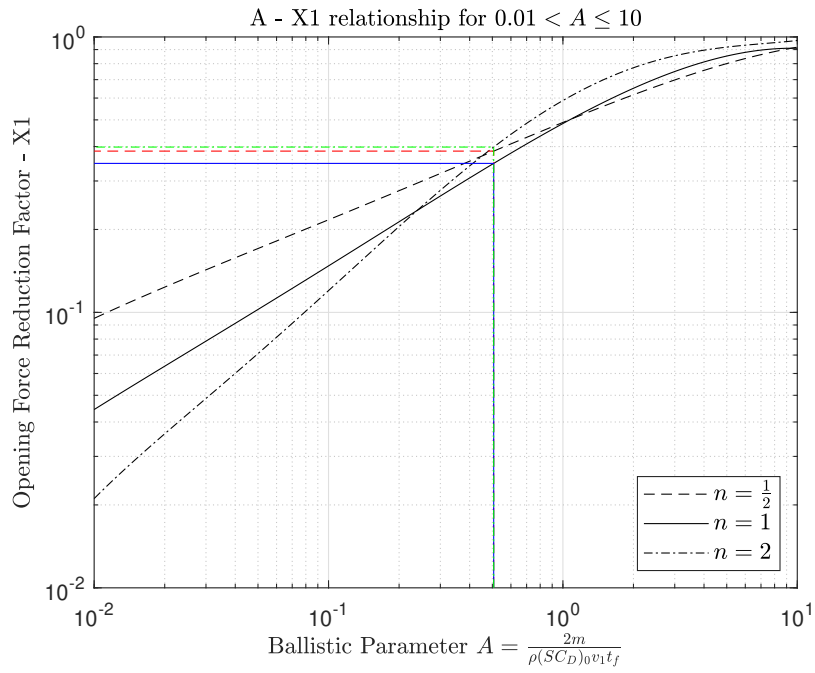
- F_{max} analytic estimation: 2348.14 N

Figure H.4: IFC 72" Iris Ultra Standard Parachute Estimation of X_1 following Pflanz Method [3]

Bibliography

[1] Sima Qian. *Historical Records*. 91 B.C.

[2] T.W. Knacke E.G. Ewing H.W. Bixby. *Recovery System Design Guide*. USAF - DEFENSE TECHNICAL INFORMATION CENTER, 1978.

[3] Theo W. Knacke. *Parachute Recovery Systems Design Manual*. Para Publishing, 1991.

[4] Robert J. Sinclair Matthew L. Zwicker. "Pack Density Limitations of Hybrid Parachutes". In: (2013). DOI: https://doi.org/10.2514/6.2013-1395.

[5] Brighenti B., Duffen S., and McGinley K. "Performance of Vented Round Parachutes - Worcester Polytechnic Institute". In: (2007).

[6] K. Stein et al. ""Aerodynamic Interaction Between Multiple Parachute Canopies". In: *Proceedings of the First MIT Conference on Computational Fluid and Solid Mechanics* (2001), pp. 968–972. DOI: https://doi.org/10.1016/B978-008043944-0/50816-7.

[7] E. Ray and D. Bretz. "Photogrammetric Analysis of CPAS Main Parachutes". In: (2011). DOI: https://doi.org/10.2514/6.2011-2538.

[8] Flight Standards Service - U.S. Department of Transportation. *Parachute Rigger Handbook*. Federal Aviation Administration (FAA), 2015. ISBN: B000WYOJ0Q.

[9] R.C. Maydew, C.W. Peterson, and K. J. Orlik-Rueckemann. "Design and Testing of High-Performance Parachutes (La Conception et les Essais des Parachutes a Hautes Performances)". In: (1991).

[10] T. Evans. *A Review of Knot Strength Testing*. http://sarrr.weebly.com/sar3-original-research/a-review-of-knot-strength-testing. 2016.

[11] M. Bibiano, F. Gracía, and R. Torres. "MIURA 1: The Reusable Soinding Rocket. Recovery and Reuseability Strategies". In: (2017). DOI: https://doi.org/10.13009/EUCASS2019-358.

[12] *Parachute Deployment*. https://chutes.nl/design-guide/deploymentsystem.html. Accessed: 25-05-2022.

[13] J. Potvin. "Universality Considerations for Graphing Parachute Opening Shock Factor Versus Mass Ratio". In: (2007). DOI: http://dx.doi.org/10.2514/1.24061.

[14] H.G. Heinrich. "A linearised theory of parachute opening dynamics". In: *The Aeronautic Journal* (1972), pp. 723–731. DOI: https://doi.org/10.1017/S0001924000044481.

[15] W.P. Ludtke. "A technique for the calculation of the opening-shock forces for several types of solid cloth parachutes". In: (1972). DOI: https://doi.org/10.2514/6.1973-477.

[16] E. Ortega and R. Flores. "Aeroelastic analysis of parachute deceleration systems with empirical aerodynamics". In: (2019). DOI: https://doi.org/10.1177/0954410019883109.

[17] D. Wolf. "Parachute Opening Shock". In: (1999). DOI: https://doi.org/10.2514/6.1999-1702.

[18] J. Lingard. "A semi-empirical theory to predict the load-time history of an inflating parachute". In: (1984). DOI: https://doi.org/10.2514/6.1984-814.

[19] G. Peek and J. Potvin. *OSCALC - Opening Shock Calculator Version 1.01 User's Manual.* https://docplayer.net/57760003-Oscalc-opening-shock-calculator-version-1-01-user-s-manual.html. 2007.

[20] Portugal Space. *European Rocketry Challenge - Design, Testing and Evaluation Guide.* https://euroc.pt/wp-content/uploads/2022/02/EuRoC2022_DTEG_V03.pdf. 2021.

[21] Festo ©. *Cilindro Redondo DSNU-S.* https://www.festo.com/media/pim/047/D15000100152047.PDF. 2022.

[22] Airgun Depot ©. *CO2 Cartridge Pressure.* URL: https://www.airgundepot.com/vault/articles/co2-cartridge-pressure/. (accessed: 2.03.2022).

[23] HARA. *How to: Ejection Charges.* URL: http://hararocketry.org/hara/wp-content/uploads/2014/05/How_To_Size_Ejection_Charges.pdf. (accessed: 5.03.2022).

[24] S. Fadala. *Blackpowder Loading Manual, 3rd Edition.* DBI Books, Inc, 1995. ISBN: 9780873491228.

[25] Weather Spark. *El clima y el tiempo promedio en todo el año en Ponte de Sôr.* URL: https://es.weatherspark.com/. (accessed: 16.04.2022).

[26] topographic-map. *Ponte de Sor.* URL: https://en-gb.topographic-map.com/maps/qwo3/Ponte-de-Sor/. (accessed: 16.04.2022).

[27] Ian Bellis. *Re-designing the three-ring release system.* https://www.flyaerodyne.com/wp-content/uploads/2017/05/Miniforce-System.pdf.

[28] EASA. *Easy Access Rules for Unmanned Aircraft Systems (Regulation (EU) 2019/947 and Regulation (EU) 2019/945).* (accessed: 22.06.2022).